The Journal of Clinical Investigation

Genomic and epigenomic *EBF1* alterations modulate *TERT* expression in gastric cancer

Manjie Xing, … , Bin Tean Teh, Patrick Tan

J Clin Invest. 2020. https://doi.org/10.1172/JCI126726.

Research Article Gastroenterology Oncology

Graphical abstract

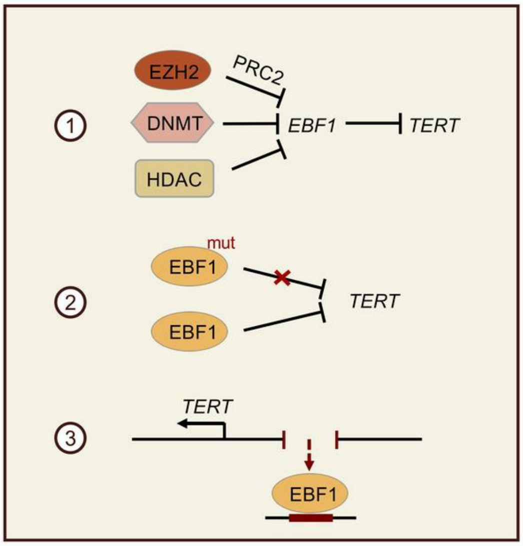
①
EZH2
PRC2
DNMT
HDAC
EBF1
TERT
②
mut
EBF1
EBF1
TERT
③
TERT
EBF1

Find the latest version:

https://jci.me/126726/pdf

Genomic and epigenomic *EBF1* alterations modulate *TERT* expression in gastric cancer

Manjie Xing,[1,2,3] Wen Fong Ooi,[2] Jing Tan,[4,5] Aditi Qamra,[2,3] Po-Hsien Lee,[6] Zhimei Li,[5] Chang Xu,[1,6] Nisha Padmanabhan,[1] Jing Quan Lim,[7] Yu Amanda Guo,[8] Xiaosai Yao,[9] Mandoli Amit,[1] Ley Moy Ng,[6] Taotao Sheng,[1,10] Jing Wang,[1] Kie Kyon Huang,[1] Chukwuemeka George Anene-Nzelu,[11,12] Shamaine Wei Ting Ho,[1,6] Mohana Ray,[13] Lijia Ma,[13] Gregorio Fazzi,[14] Kevin Junliang Lim,[1] Giovani Claresta Wijaya,[5] Shenli Zhang,[1] Tannistha Nandi,[2] Tingdong Yan,[1] Mei Mei Chang,[8] Kakoli Das,[1] Zul Fazreen Adam Isa,[2] Jeanie Wu,[1] Polly Suk Yean Poon,[2] Yue Ning Lam,[2] Joyce Suling Lin,[2] Su Ting Tay,[1] Ming Hui Lee,[1] Angie Lay Keng Tan,[1] Xuewen Ong,[1] Kevin White,[13,15] Steven George Rozen,[1,16] Michael Beer,[17,18] Roger Sik Yin Foo,[11,12] Heike Irmgard Grabsch,[14,19] Anders Jacobsen Skanderup,[8] Shang Li,[1,20] Bin Tean Teh,[1,5,6,9,16,20] and Patrick Tan[1,2,6,16,21,22,23]

[1]Cancer and Stem Cell Biology Program, Duke-NUS Medical School, Singapore. [2]Cancer Therapeutics and Stratified Oncology, Genome Institute of Singapore, Singapore. [3]NUS Graduate School for Integrative Sciences and Engineering, National University of Singapore, Singapore. [4]State Key Laboratory of Oncology in South China, Sun Yat-Sen University Cancer Center, Guangzhou, China. [5]Laboratory of Cancer Epigenome, Department of Medical Sciences, National Cancer Centre, Singapore. [6]Cancer Science Institute of Singapore, National University of Singapore, Singapore. [7]Lymphoma Genomic Translational Research Laboratory, Cellular and Molecular Research, National Cancer Centre Singapore, Singapore. [8]Computational and Systems Biology, Agency for Science Technology and Research, Genome Institute of Singapore. [9]Institute of Molecular and Cell Biology, Singapore. [10]Department of Biochemistry, National University of Singapore, Singapore. [11]Cardiovascular Research Institute, National University Health System, Singapore. [12]Human Genetics, Genome Institute of Singapore, Singapore. [13]Institute for Genomics and Systems Biology, University of Chicago, Chicago, Illinois, USA. [14]Department of Pathology, GROW School for Oncology and Developmental Biology, Maastricht University Medical Center, Maastricht, Netherlands. [15]Tempus Labs, Chicago, Illinois, USA. [16]SingHealth/Duke-NUS Institute of Precision Medicine, National Heart Centre Singapore, Singapore. [17]McKusick-Nathans Institute of Genetic Medicine, Johns Hopkins Medicine, and [18]Department of Biomedical Engineering, Johns Hopkins University, Baltimore, Maryland, USA. [19]Pathology and Data Analyticis, Leeds Institute of Medical Research at St. James's, University of Leeds, Leeds, United Kingdom. [20]Department of Physiology, Yong Loo Lin School of Medicine, National University of Singapore, Singapore. [21]Cellular and Molecular Research, National Cancer Centre, Singapore. [22]Singapore Gastric Cancer Consortium, Singapore. [23]Biomedical Research Council, Agency for Science, Technology and Research, Singapore.

Transcriptional reactivation of telomerase catalytic subunit (*TERT*) is a frequent hallmark of cancer, occurring in 90% of human malignancies. However, specific mechanisms driving *TERT* reactivation remain obscure for many tumor types and in particular gastric cancer (GC), a leading cause of global cancer mortality. Here, through comprehensive genomic and epigenomic analysis of primary GCs and GC cell lines, we identified the transcription factor early B cell factor 1 (*EBF1*) as a *TERT* transcriptional repressor and inactivation of *EBF1* function as a major cause of *TERT* upregulation. Abolishment of *EBF1* function occurs through 3 distinct (epi)genomic mechanisms. First, *EBF1* is epigenetically silenced via DNA methyltransferase, polycomb-repressive complex 2 (PRC2), and histone deacetylase activity in GCs. Second, recurrent, somatic, and heterozygous *EBF1* DNA–binding domain mutations result in the production of dominant-negative *EBF1* isoforms. Third, more rarely, genomic deletions and rearrangements proximal to the *TERT* promoter remobilize or abolish *EBF1*-binding sites, derepressing *TERT* and leading to high *TERT* expression. *EBF1* is also functionally required for various malignant phenotypes in vitro and in vivo, highlighting its importance for GC development. These results indicate that multimodal genomic and epigenomic alterations underpin *TERT* reactivation in GC, converging on transcriptional repressors such as *EBF1*.

Introduction

Gastric cancer (GC) is a leading cause of global cancer mortality (1), with a particularly high prevalence in East Asia. With the exception of Japan and South Korea, where the absolute GC incidence is sufficiently high to enable cost-effective endoscopic screening, today most patients with GC are diagnosed at advanced stages of the disease, resulting in low overall survival (2). Targeted agents approved for clinical use in GC include trastuzumab for human epidermal growth factor receptor 2–positive (HER2-positive) GC (3), ramicurumab (VEGFR2) (4), and immuno-oncology agents such as pembrolizumab (5) and nivolumab (6). However, these treatments are typically only effective in small subsets of patients with GC, and clinical trials evaluating alternative GC molecular targets have proved disappointing (7–10). Investigating the basic mechanisms of GC tumorigenesis may therefore elucidate the early steps in gastric malignancy and lead to new therapeutic interventions.

Reactivation of telomerase is a pivotal step in cancer initiation. Telomere sequences at chromosome ends are lost during successive rounds of DNA replication, and critically short telomeres can induce cellular senescence and apoptosis. Telomerase is an RNA-dependent DNA polymerase consisting of an RNA component (*TERC*) and a protein catalytic subunit (*TERT*) that can lengthen a chromosome's telomeres. *TERT* is normally expressed in human stem and germ cells but is silenced in differ-

---

Authorship note: MX, WFO, and JT contributed equally to this work.

Conflict of interest: The authors have declared that no conflict of interest exists.

Submitted: December 10, 2018; **Accepted:** February 26, 2020; **Published:** May 4, 2020.

Reference information: *J Clin Invest*. https://doi.org/10.1172/JCI126726.

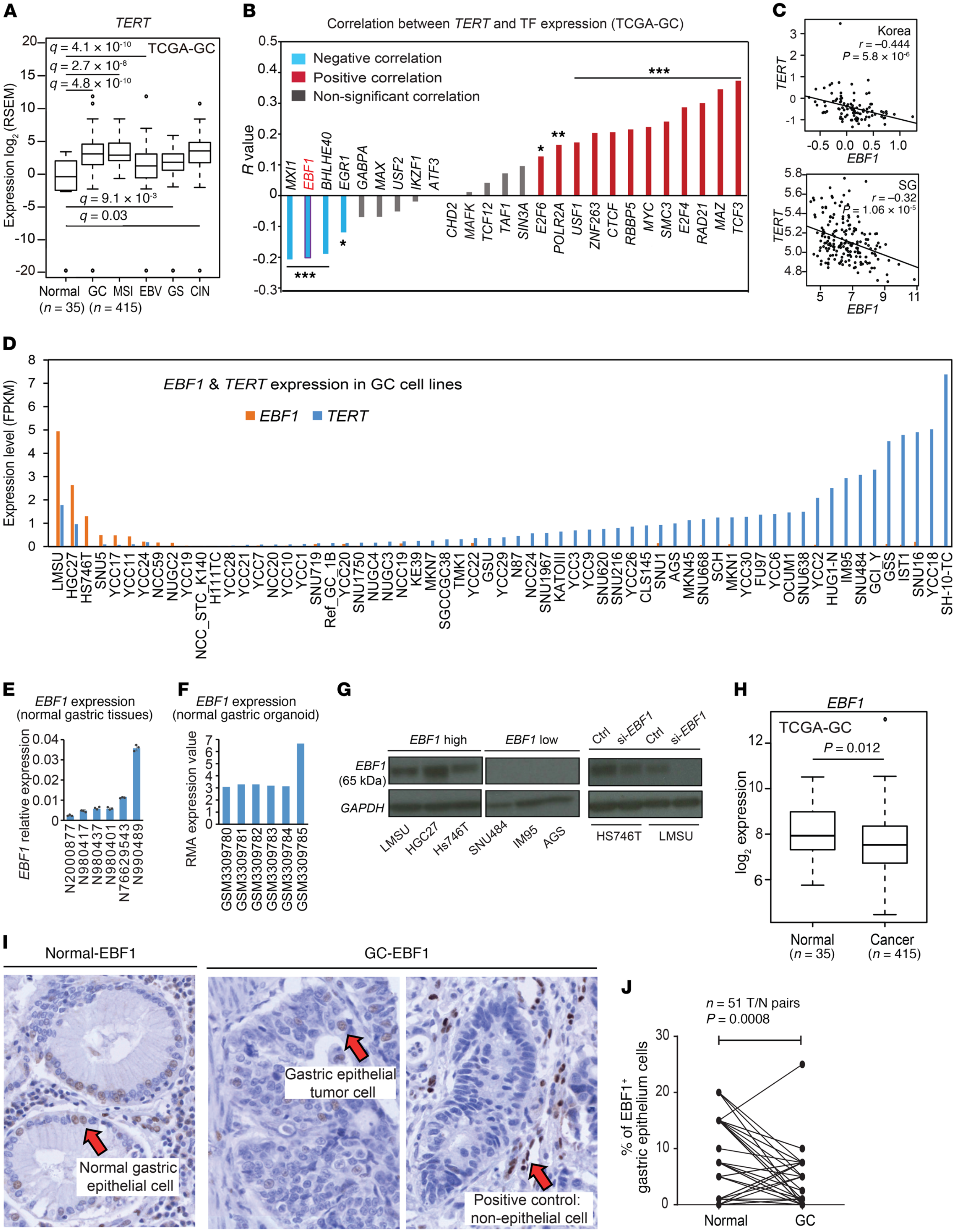
A
TERT
TCGA-GC
$q = 4.1 \times 10^{-10}$
$q = 2.7 \times 10^{-8}$
$q = 4.8 \times 10^{-10}$
$q = 9.1 \times 10^{-3}$
$q = 0.03$
Expression $\log_2$ (RSEM)
20
15
10
5
0
-5
-10
-20
Normal GC MSI EBV GS CIN
(n = 35) (n = 415)
B
Correlation between TERT and TF expression (TCGA-GC)
Negative correlation
Positive correlation
Non-significant correlation
R value
0.5
0.4
0.3
0.2
0.1
0
-0.1
-0.2
-0.3
***
*
**
***
MXI1
EBF1
BHLHE40
EGR1
GABPA
MAX
USF2
IKZF1
ATF3
CHD2
MAFK
TCF12
TAF1
SIN3A
E2F6
POLR2A
USF1
ZNF263
CTCF
RBBP5
MYC
SMC3
E2F4
RAD21
MAZ
TCF3
C
Korea
r = –0.444
$P = 5.8 \times 10^{-6}$
TERT
EBF1
3
2
1
0
-1
-0.5 0.0 0.5 1.0
SG
r = –0.32
$P = 1.06 \times 10^{-5}$
5.8
5.6
5.4
5.2
5.0
4.8
5 7 9 11
D
EBF1 & TERT expression in GC cell lines
EBF1
TERT
Expression level (FPKM)
8
7
6
5
4
3
2
1
0
LMSU
HGC27
HS746T
SNU5
YCC17
YCC11
YCC24
NCC59
NUGC2
YCC19
NCC_STC_K140
H111TC
YCC28
YCC21
YCC7
NCC20
YCC10
YCC1
SNU719
Ref_GC_1B
YCC20
SNU1750
NUGC4
NUGC3
NCC19
KE39
MKN7
SGCCGC38
TMK1
YCC22
GSU
YCC29
N87
NCC24
SNU1967
KATOIII
YCC3
YCC9
SNU620
SNU216
YCC26
CLS145
SNU1
AGS
MKN45
SNU668
SCH
MKN1
YCC30
FU97
YCC6
OCUM1
SNU638
YCC2
HUG1-N
IM95
SNU484
GCI_Y
GSS
IST1
SNU16
YCC18
SH-10-TC
E
EBF1 expression
(normal gastric tissues)
EBF1 relative expression
0.04
0.03
0.02
0.01
0
N2000877
N980417
N980437
N980401
N76629543
N990489
F
EBF1 expression
(normal gastric organoid)
RMA expression value
7
6
5
4
3
2
1
0
GSM3309780
GSM3309781
GSM3309782
GSM3309783
GSM3309784
GSM3309785
G
EBF1 high
EBF1 low
Ctrl
si-EBF1
Ctrl
si-EBF1
EBF1
(65 kDa)
GAPDH
LMSU
HGC27
Hs746T
SNU484
IM95
AGS
HS746T
LMSU
H
EBF1
TCGA-GC
P = 0.012
$\log_2$ expression
12
10
8
6
Normal
(n = 35)
Cancer
(n = 415)
I
Normal-EBF1
GC-EBF1
Normal gastric
epithelial cell
Gastric epithelial
tumor cell
Positive control:
non-epithelial cell
J
n = 51 T/N pairs
P = 0.0008
% of EBF1⁺
gastric epithelium cells
30
20
10
0
Normal
GC

Figure 1. *EBF1* TF expression is negatively associated with *TERT*. (**A**) Expression of *TERT* in normal gastric ($n = 35$) and GC samples ($n = 415$) from TCGA consortium. Q values were determined by Wilcoxon's rank-sum test with FDR multiple testing correction. RSEM, RNA-Seq by expectation-maximization (https://github.com/deweylab/RSEM). (**B**) Correlation of mRNA levels between *TERT* and TFs (ENCODE ChIP-Seq database) at genomic regions flanking the *TERT* TSS. Correlation coefficients were computed using the normalized expression matrix from TCGA. $^{*}Q < 0.05$, $^{**}Q < 0.01$, and $^{***}Q < 0.001$, by Pearson's correlation test with FDR multiple testing correction. (**C**) A significant negative correlation was found between *TERT* and *EBF1* mRNA levels in the South Korean and Singapore cohorts. Top: microarray data for 96 GC samples from the Korean cohort (median-centered, log-transformed). Bottom: microarray data for 185 GC samples from the Singapore (SG) cohort ($\log_2$ expression level). P values were determined by Pearson's correlation test. (**D**) Graph shows *EBF1* and *TERT* expression levels based on RNA-Seq data for 63 GC lines. FPKM, fragments per kilobase per million mapped reads. (**E**) TaqMan qPCR validation of *EBF1* expression levels using in-house normal stomach tissues. (**F**) *EBF1* expression levels in normal gastric organoids (microarray). RMA, robust multiarray average. (**G**) Western blot analysis of EBF1 protein expression in GC lines. Ctrl, control. (**H**) Expression of *EBF1* in normal gastric ($n = 35$) and GC samples ($n = 415$) from TCGA. P value was determined by Wilcoxon's rank sum test. (**I**) EBF1 immunohistochemistry for GC tissues and normal gastric epithelium. Left: normal gastric epithelium with EBF1 expression (brown); middle: GC cells with EBF1 expression in 15% of the tumor cells (brown); right: intestinal-type GC cells with complete loss of EBF1 expression, endothelial cells and lymphocytes in the tumor stroma were EBF1^{+} (brown). Original magnification, x40. Red arrows indicate stained cells. (**J**) Distribution of immunohistochemical scores for EBF1 protein expression in 51 GCs and matched normal tissues, connected by black lines. P value was determined by 2-sided t test. (**A** and **H**) For the box-and-whisker plots, the lines within boxes indicate the median, the bounds of the boxes indicate the upper and lower quartiles, the whiskers indicate the minimum and maximum values, and the separated points indicate outliers.

entiated somatic cells and transcriptionally reactivated in up to 90% of human malignancies (11, 12). *TERT* reactivation is a driver of oncogenic alteration, contributing to cellular transformation, immortalization, and oncogenic development in many cancer types. Clinically, high *TERT* expression levels have been associated with aggressive disease. In GC specifically, high *TERT* levels have been associated with poor prognosis, advanced disease stage, and lymphatic metastasis and invasion (13–15).

Despite their importance, the cellular mechanisms driving the transcriptional reactivation of *TERT* in cancers remain poorly described, particularly in the case of GC. In certain cancers, *TERT* promoter somatic mutations (C250T and C228T) have been described as a major mechanism of telomerase reactivation (16, 17), however, these promoter hotspot mutations appear to be infrequent in GC (<1%) (18). Besides promoter point mutations, large-scale genomic alterations such as enhancer hijacking (19) and copy number alterations (20) affecting *TERT* have been reported, and at the *trans*-regulatory level, oncogenic transcriptional activators (*Sp1*, *c-MYC*, *AP2*, and *HIF-1*) and tumor-suppressive transcriptional repressors (*p53*, *Menin*, and *WT1*) may also regulate *TERT* (21). To date, however, specific mechanisms underlying *TERT* reactivation in GC remain largely unknown.

In this study, we focused on investigating molecular processes that govern *TERT* expression in GC. By integrating genomic data from primary GCs and GC cell lines, we identified the early B cell factor 1 (*EBF1*) transcription factor (TF) as a candidate *TERT* repressor and validated its function through in vitro and in vivo studies. We provide evidence that in GC, *EBF1* function is suppressed by various mechanisms, including epigenetic inactivation, dominant-negative mutations, and large-scale genomic alterations affecting *EBF1 cis*-binding regions at the *TERT* promoter. *EBF1* inhibition may therefore contribute to *TERT* reexpression and activity in GC.

Results

EBF1 TF expression is negatively associated with TERT. To investigate *TERT* expression in GC, we queried RNA-Seq profiles of primary GCs from The Cancer Genome Atlas (TCGA) consortium ($n = 415$ GCs, $n = 35$ normal samples), in-house databases of primary tumors ($n = 18$ tumor/normal [T/N] pairs of GCs), and GC cell lines ($n = 63$). We found that *TERT* was significantly upregulated in GC samples compared with normal samples ($P = 1.9$, Figure 1A × 10^{-10}; Supplemental Figure 1A; supplemental material available online with this article; https://doi.org/10.1172/JCI126726DS1) and exhibited variable expression across GC lines (Supplemental Figure 1B). *TERT* overexpression was greater in GCs with chromosomal instability (CIN) or microsatellite instability (MSI) compared with genome-stable (GS) or EBV-positive tumors (Figure 1A). These results are consistent with previous independent studies reporting increased *TERT* expression in GC (see Discussion and refs. 22–24). To determine the prevalence of *TERT* promoter point mutations in GC, we surveyed whole-genome sequences (WGSs) of 212 GCs and matched normal samples (25) but detected no mutations at previously reported *TERT* mutational hotspots (C228T and C250T), consistent with previous reports that *TERT* promoter hotspot mutations are rare in GC (18).

We sought to identify *trans*-acting TFs that regulate *TERT* in GC. Hypothesizing that *TERT*-regulatory TFs should exhibit genomic occupancy of the *TERT* promoter region and also systematic relationships with *TERT* expression, we proceeded to correlate *TERT* expression levels (inferred from TCGA GCs) against the expression patterns of 26 TFs predicted to bind around the *TERT* transcription start site (TSS) (± 10 kb). These 26 factors were identified on the basis of their predicted ability to bind to the *TERT* promoter region using ChIP-Seq data from the ENCODE ChIP-Seq database (https://genome.ucsc.edu/ENCODE/3). Confirming the utility of this approach, this analysis reidentified several previously known *TERT* regulators, such as *MYC* (*TERT* activator) and *MXI1* (*TERT* repressor) (26, 27). Notably, we observed that *TERT* expression levels were negatively correlated with the *EBF1* TF, ranking second in significance among the putative *TERT*-regulatory TFs ($R = -0.20$, $P = 1.2 \times 10^{-5}$; Figure 1B). We extended our analysis to 2 other GC expression microarray cohorts and again observed similar significant negative correlations between *TERT* and *EBF1*, thus validating this observation in independent cohorts (Figure 1C).

Historically studied as a TF in B-lineage immune cells, *EBF1* expression has been recently described in solid tumors such as breast cancer, cholangiocarcinoma, and glioblastoma (28, 29). To explore *EBF1* expression in stomach tissues, we mined the Genotype–Tissue Expression (GTEx) database (https://www.gtexportal.org/home/) and observed that *EBF1* is expressed in many human tissues and cell types including stomach (Supple-

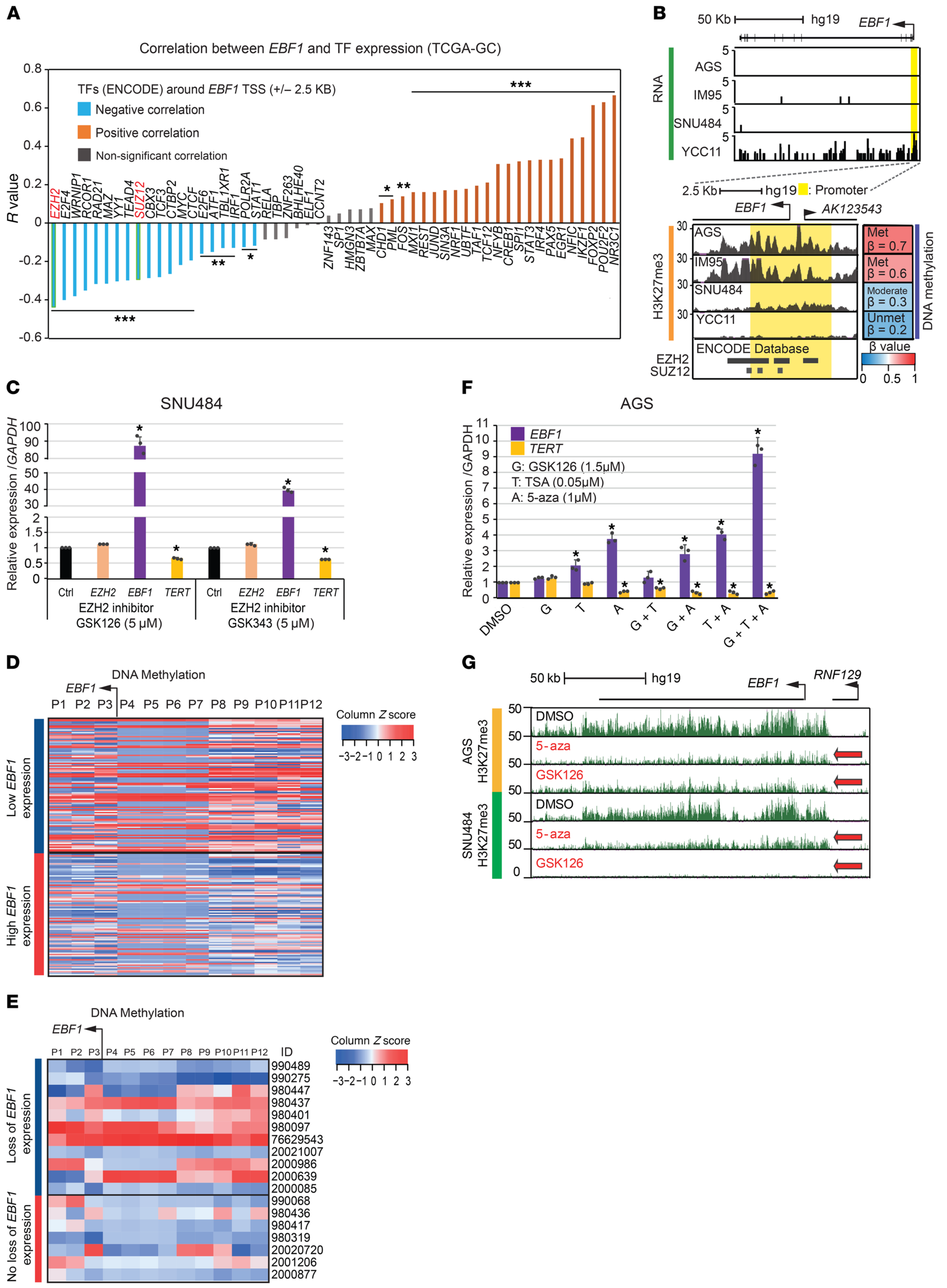
A
Correlation between EBF1 and TF expression (TCGA-GC)
TFs (ENCODE) around EBF1 TSS (+/– 2.5 KB)
Negative correlation
Positive correlation
Non-significant correlation
R value
EZH2 E2F4 WRNIP1 RCOR1 RAD21 MAZ YY1 TEAD4 SUZ12 CBX3 TCF3 CTBP2 MYC CTCF E2F6 ATF1 TBL1XR1 IRF1 POLR2A STAT1 RELA TBP ZNF263 BHLHE40 ELF1 CCNT2
ZNF143 SP1 HMGN3 ZBTB7A MAX CHD1 PML FOS MXI1 REST JUND SIN3A NRF1 UBTF TAF1 TCF12 NFYB CREB1 SPI1 STAT3 IRF4 PAX5 EGR1 NFIC IKZF1 FOXP2 POU2F2 NR3C1
***
**
*
B
50 Kb
hg19
EBF1
RNA
AGS
IM95
SNU484
YCC11
2.5 Kb
hg19
: Promoter
AK123543
H3K27me3
ENCODE Database
EZH2
SUZ12
Met β = 0.7
Met β = 0.6
Moderate β = 0.3
Unmet β = 0.2
DNA methylation
β value
0 0.5 1
C
SNU484
Relative expression /GAPDH
Ctrl EZH2 EBF1 TERT
EZH2 inhibitor GSK126 (5 μM)
EZH2 inhibitor GSK343 (5 μM)
D
DNA Methylation
EBF1
P1 P2 P3 P4 P5 P6 P7 P8 P9 P10 P11 P12
Low EBF1 expression
High EBF1 expression
Column Z score
−3 −2 −1 0 1 2 3
E
DNA Methylation
EBF1
P1 P2 P3 P4 P5 P6 P7 P8 P9 P10 P11 P12
ID
990489
990275
980447
980437
980401
980097
76629543
20021007
2000986
2000639
2000085
990068
980436
980417
980319
20020720
2001206
2000877
Loss of EBF1 expression
No loss of EBF1 expression
Column Z score
−3 −2 −1 0 1 2 3
F
AGS
EBF1
TERT
G: GSK126 (1.5μM)
T: TSA (0.05μM)
A: 5-aza (1μM)
Relative expression /GAPDH
DMSO G T A G + T G + A T + A G + T + A
G
50 kb
hg19
EBF1
RNF129
AGS H3K27me3
SNU484 H3K27me3
DMSO
5-aza
GSK126

Figure 2. *EBF1* is transcriptionally silenced in GC via repressive histone modifications and DNA methylation. (**A**) Correlation of mRNA expression levels between *EBF1* and TFs at genomic regions flanking the *EBF1* TSS. Correlation coefficients were computed using the normalized expression matrix from TCGA ($n = 415$ tumors, $n = 35$ normal samples). *$Q < 0.05$, **$Q < 0.01$, and ***$Q < 0.001$, by Pearson's correlation test with FDR multiple testing correction. (**B**) H3K27me3, EZH2, and SUZ12 signals flanking the *EBF1* TSS. Top: RNA-Seq tracks depict *EBF1* expression in GC lines. Bottom left: H3K27me3, EZH2, and SUZ12 enrichment. Yellow bar indicates the *EBF1* promoter (TSS ± 2.5 kb). Bottom right: DNA methylation levels of GC lines. Colored graph shows the average β value of 12 CpG probes in the 5′-UTR and TSS of *EBF1*. EZH2 and SUZ12 ChIP-Seq data are from the ENCODE database. Layered signals from multiple cell lines are shown for EZH2 (H1 human embryonic stem cells [H1-hESCs], human mammary epithelial cells [HMECs], human umbilical vein endothelial cells [HUVECs], normal human astrocytes [NHAs], normal human epidermal keratinocytes [NHEKs], and normal human lung fibroblasts [NHLFs]). The SUZ12 profile is from H1-hESCs. (**C**) *EZH2* and *EBF1* expression levels in SNU484 cells after drug treatment. (**D**) DNA methylation 450K array data from TCGA. Data were plotted for the top and bottom 25th percentiles of *EBF1*-expressing samples ($n = 191$). (**E**) In-house DNA methylation 450K array data for 18 T/N GC pairs. Heatmap shows GCs with or without loss of *EBF1*. (**D** and **E**) Data are from 12 CpG probes in the 5′-UTR and TSS region of *EBF1*. (**F**) Response patterns of *EBF1* and *TERT* mRNA levels following drug treatments. (**C** and **F**) Control cells were treated with DMSO. *$Q < 0.05$, by 2-sided t test with FDR multiple testing correction. qPCR results are shown as the mean ± SD of technical triplicates. All data are representative of 3 independent experiments. (**G**) H3K27me3 enrichment at the *EBF1* locus from GC cell lines with DMSO, 5-aza, and GSK126 treatment. Red arrows indicate a decrease in H3K27me3 enrichment.

mental Figure 1C and ref. 30). To confirm that *EBF1* is expressed in GC epithelial cells, we compared *EBF1* and *TERT* RNA-Seq expression levels across a panel of 63 GC cell lines. GC cell lines with high *EBF1* expression exhibited no or low *TERT* transcript levels, whereas the majority of cell lines lacking *EBF1* expression displayed high *TERT* expression (Figure 1D). *EBF1* mRNA expression in stomach was further confirmed by TaqMan quantitative PCR (qPCR) analysis of a diverse collection of gastric-related samples, including primary normal gastric tissues ($n = 6$), GC cell lines ($n = 4$); gene expression analysis of TCGA normal gastric tissues (RNA-Seq, $n = 39$); data from 2 additional public data sets (31, 32); and analysis of normal gastric organoids ($n = 6$) (Figure 1, E and F, Supplemental Figure 1, D–G, and ref. 33) . To confirm EBF1 expression at the protein level, we performed Western blotting using anti-EBF1 antibodies validated by both predicted protein size (Figure 1G, left and middle) and siRNA-knockdown assays (Figure 1G, right). We confirmed endogenous EBF1 protein expression in cell lines showing high *EBF1* transcript levels and low EBF1 protein expression in cell lines expressing low levels of *EBF1* transcripts.

Compared with normal gastric tissues, *EBF1* transcripts were significantly downregulated in GC (TCGA samples, $P = 0.012$; Figure 1H) — a pattern opposite that of *TERT* transcript levels. To confirm EBF1 protein expression in primary GCs, we performed EBF1 immunohistochemical analysis on a panel of GCs and matched normal tissues. This analysis revealed EBF1 expression in scattered nuclei of normal gastric epithelium and GC cells (Figure 1I), ranging from 0% to 25% of cells (Figure 1J). Similar to the gene expression data, primary GCs exhibited significantly lower EBF1 immunohistochemical scores than did normal gastric tissues ($P = 0.0008$, $n = 51$ T/N pairs; Figure 1J). When compared with GCs with different clinicopathological characteristics, *EBF1* loss was more frequent in diffuse-type GCs and poorly differentiated GCs ($P = 0.001$ and $P = 0.002$ respectively, $n = 109$ patients; Supplemental Table 1). We also observed a trend toward more frequent *EBF1* loss in patients with a higher number of lymph node metastases ($P = 0.052$, $n = 109$ patients; Supplemental Table 1).

EBF1 is transcriptionally silenced in GC via repressive histone modifications and DNA methylation. To explore potential mechanisms underlying *EBF1* downregulation in GC, we found a promoter occupancy/expression correlation similar to that depicted in Figure 1B, but this time analyzing the *EBF1* instead of the *TERT* promoter region. Correlation of TFs predicted to bind the *EBF1* promoter region (± 2.5 kb) to *EBF1* mRNA expression levels revealed a strong negative correlation of *EBF1* with 2 polycomb-repressive complex 2 (PRC2) subunits: *EZH2* ($R = -0.44$, $P < 0.00001$) and *SUZ12* ($R = -0.29$, $P = 2.4 \times 10^{-10}$) (Figure 2A). We queried EZH2 and SUZ12 ChIP-Seq data from the ENCODE database and found EZH2 and SUZ12 occupancy at the *EBF1* promoter in various cell types (Figure 2B). As PRC2 is known to catalyze the H3K27me3-repressive histone mark, we performed H3K27me3 ChIP-Seq analysis and confirmed H3K27me3 enrichment at the *EBF1* TSS locus in *EBF1*-low (AGS, IM95, and SNU484) but not *EBF1*-high GC cells (YCC11) (Figure 2B). Given that histone modifications and DNA methylation often cooperate to regulate gene expression (34), we also evaluated DNA methylation levels at the *EBF1* promoter using Illumina 450K DNA Methylation Arrays. We found that *EBF1*-low cell lines had high to moderate levels of *EBF1* promoter DNA methylation (high, AGS and IM95; moderate, SNU484), whereas the *EBF1*-high cell line YCC11 showed no *EBF1* promoter DNA methylation.

We explored whether targeting EZH2, the catalytic subunit of PRC2, might reactivate *EBF1*. Knockdown of *EZH2* by siRNA in the GC lines AGS and SNU484 caused a 3.2- to 7.5-fold increase in *EBF1* mRNA levels (Supplemental Figure 2, A and B). We then tested the effects of EZH2 pharmacologic inhibition using 2 distinct EZH2-inhibitory compounds, GSK126 and GSK343 (Figure 2C and Supplemental Figure 2C). In SNU484 cells, EZH2 inhibition was accompanied by a 40- to 87-fold increase in *EBF1* expression levels. However, in AGS cells, EZH2 monoinhibition did not induce similarly strong changes in *EBF1* expression. To further explore this observation, we noted recent studies have shown that multiple epigenetic pathways often act in a coordinated and combinatorial manner to repress target promoters. For example, EZH2 requires histone deacetylases (HDACs) to silence targets (35), and EZH2 can directly control DNA methylation by recruiting DNA methyltransferase (DNMT) (34). We thus explored whether *EBF1* might also be regulated by DNMTs and HDACs. Examination of methylation array data from 191 GCs from the TCGA consortium revealed higher levels of *EBF1* promoter DNA methylation in GCs with low *EBF1* expression (i.e., higher β values), whereas GCs with high *EBF1* expression exhibited lower DNA methylation levels (i.e., lower β values; Figure 2D). We observed a similar trend in a pairwise fashion in an in-house cohort of GCs with matched normal samples ($n = 18$ T/N pairs; Figure 2E and Supplemental Figure 2D; the same 12 CpG probes were measured in both cohorts). The degree of the β value methylation differences is fully consistent with definitions of hypermethylation by other independent stud-

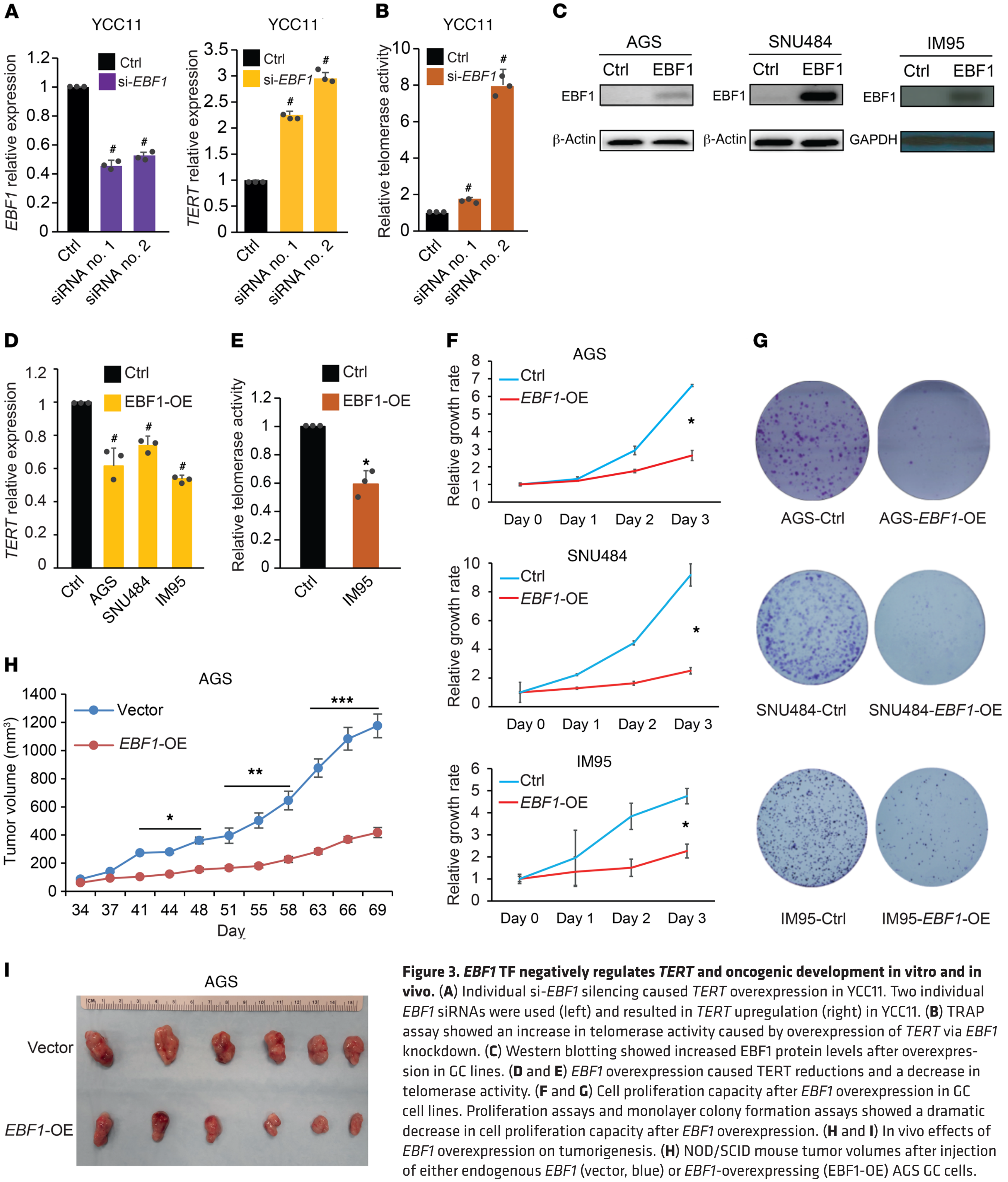

Figure 3. *EBF1* TF negatively regulates *TERT* and oncogenic development in vitro and in vivo. (**A**) Individual si-*EBF1* silencing caused *TERT* overexpression in YCC11. Two individual *EBF1* siRNAs were used (left) and resulted in *TERT* upregulation (right) in YCC11. (**B**) TRAP assay showed an increase in telomerase activity caused by overexpression of *TERT* via *EBF1* knockdown. (**C**) Western blotting showed increased EBF1 protein levels after overexpression in GC lines. (**D** and **E**) *EBF1* overexpression caused TERT reductions and a decrease in telomerase activity. (**F** and **G**) Cell proliferation capacity after *EBF1* overexpression in GC cell lines. Proliferation assays and monolayer colony formation assays showed a dramatic decrease in cell proliferation capacity after *EBF1* overexpression. (**H** and **I**) In vivo effects of *EBF1* overexpression on tumorigenesis. (**H**) NOD/SCID mouse tumor volumes after injection of either endogenous *EBF1* (vector, blue) or *EBF1*-overexpressing (EBF1-OE) AGS GC cells. Tumor volumes were measured every 3 days. $n = 6$ mice per group. (**I**) Image of harvested tumors after an experimental period of 10 weeks. Tumor sizes are shown in centimeters. $^{\#}Q < 0.05$, by 2-sided t test with FDR multiple testing correction (**A**, **B**, and **D**). $^{*}P < 0.05$, $^{**}P < 0.01$, and $^{***}P < 0.001$, by 2-sided t test (**E**, **F**, and **H**). Error bars indicate the SD. RT-PCR results are shown as the mean ± SD of technical triplicates. All data are representative of 3 independent experiments.

ies (36, 37). For orthogonal validation of the β value DNA methylation levels, we performed quantitative DNA methylation assays (MethylLight) in 8 T/N pairs to determine *EBF1* promoter DNA methylation levels (4 pairs with the highest methylation levels in GCs and 4 pairs randomly selected from GCs with low methylation levels; Supplemental Figure 2E). The quantitative DNA methylation results were concordant with patterns from the 450K DNA methylation β values. Taken collectively, these results suggest that approximately half (40%–55%) of primary GCs with loss of *EBF1* expression have high levels of *EBF1* promoter methylation.

To determine whether epigenetic drug combinations might affect *EBF1* expression, we performed single-, double-, and triple-agent combination treatments of AGS and SNU484 cells with EZH2 inhibitors (GSK126), DNMT inhibitors (5-aza-2′-deoxycytidine [5-aza]), and the HDAC inhibitor trichostatin A (TSA). Treatment of AGS and SNU484 cells with 5-aza caused reexpression of *EBF1* that was approximately 4-fold and 22-fold over levels in control cells, respectively (Figure 2F and Supplemental Figure 2F), suggesting that the magnitude of *EBF1* reexpression induced by 5-aza is cell line specific, which is supported by an independent study of GC cell lines (38). For HDAC inhibition, similar *EBF1* increases were achieved by treatment with either TSA or vorinostat, a more specific HDAC inhibitor (Supplemental Figure 2G and ref. 39). Notably, compared with single-agent treatments, combinatorial epigenetic therapies consistently induced substantially higher levels of *EBF1* expression, demonstrating that *EBF1* is inactivated in GC through diverse epigenetic pathways (PRC2, DNA methylation, and HDAC). Supporting this hypothesis, in AGS cells a triple combination of epigenetic therapies (5-aza plus TSA plus GSK126) induced the most dramatic *EBF1* upregulation relative to single- and dual-agent treatments (Figure 2F).

We also asked whether epigenetic treatment affected *EBF1*-associated histone modifications and/or DNA methylation. Using H3K27me3 ChIP-Seq, we confirmed decreased H3K27me3 signals at the *EBF1* locus after treatment with either GSK126 or 5-aza in 2 cell lines (Figure 2G). Quantitative DNA methylation analysis of both cell lines before and after 5-aza treatment also confirmed significant decreases in DNA methylation levels after treatment with 5-aza but not GSK126 (Supplemental Figure 2H). However, we did not observe convincing alterations in H3K27ac signals after epigenetic treatment (Supplemental Figure 2I). It is possible that our experimental conditions and selection time points may have been too short to observe changes in H3K27ac or, alternatively, that inhibition of EZH2 (by GSK126) or DMNT (by 5-aza) may not be sufficient to alter H3K27ac patterns. Taken collectively, these results suggest that *EBF1* is transcriptionally silenced in GC through a combination of repressive histone modifications and DNA methylation.

Besides the *EBF1* promoter, we also investigated distal *cis*-regulatory element regions upstream and downstream of *EBF1* (TSS +100 kb/–1000 kb). We identified 43 potential enhancers associated with the *EBF1* locus. Of these 43, we found that 5 predicted enhancers (Supplemental Figure 2J, blue highlights) had differential H3K27ac signals between *EBF1*-high cell lines (LMSU and Hs746T) and *EBF1*-low cell lines (AGS and SNU484) ($P < 0.05$, 1-sided Student's t test). Supporting their designation as enhancer elements, these 5 enhancers were also associated with increased H3K4me1 and ATAC-Seq (assay for transposase-accessible chromatin using sequencing) signals in *EBF1*-high cell lines, but not in *EBF1*-low cell lines, and 3 of these enhancers exhibited significant interactions with the *EBF1* promoter in public databases of Promoter Capture Hi-C (pcHi-C) data (Supplemental Figure 2J; arc lines; $P < 0.01$; promoter/capture point: green bar; ref. 40).

The EBF1 TF negatively regulates TERT and oncogenic development in vitro and in vivo. Consistent with *EBF1* being a *TERT* repressor, enhancement of *EBF1* reexpression by combinatorial epigenetic therapies also caused *TERT* silencing in both cell lines (Figure 2F and Supplemental Figure 2F). To specifically test whether *EBF1* regulates *TERT*, siRNA-mediated depletion of endogenous *EBF1* using either pooled or independent *EBF1* siRNAs in YCC11 cells, which express high *EBF1* levels, resulted in 2.3- to 3-fold increases in *TERT* RNA levels, as determined by TaqMan qPCR assays (Figure 3A and Supplemental Figure 3A). Notably, this degree of *TERT* induction is comparable to expression levels associated with *TERT* promoter hotspot mutations (41). Using telomeric repeat amplification protocol (TRAP) assays, we also confirmed that *EBF1* knockdown caused 1.8- to 7.9-fold increases in telomerase activity (Figure 3B). These results were replicated and confirmed in 2 additional GC cell lines (Hs746T and HGC27), each using 2 independent *EBF1* shRNAs (Supplemental Figure 3B). In the reciprocal experiment, we induced overexpression of *EBF1* in AGS, SNU484, and IM95 cells, which express low or no *EBF1*. Western blotting confirmed increased levels of *EBF1* protein in the *EBF1*-transduced cell lines (Figure 3C), and *EBF1* overexpression resulted in a 26% to 46% decrease in *TERT* mRNA levels (Figure 3D). Similarly, using TRAP assays, we confirmed that *EBF1* overexpression caused a 30% to 40% decrease in telomerase activity (Figure 3E and Supplemental Figure 3C). These findings suggest that *EBF1* is a negative regulator of *TERT* in GC.

To assess whether *EBF1* plays a functional role in GC, we performed proliferation and monolayer colony formation assays and found that overexpression of *EBF1* in multiple cell lines dramatically reduced cellular proliferation and monolayer colony formation (Figure 3, F and G). In vivo, we tested NOD/SCID xenograft mice injected with AGS cells with or without *EBF1* overexpression. After 41 days, the tumors formed from *EBF1*-overexpressing GC cells were significantly smaller than those formed from control cells (Figure 3, H and I). The tumor growth–inhibiting effect of *EBF1* was sustained throughout the entire experimental period of approximately 10 weeks. To identify biological pathways affected by *EBF1* overexpression, we sequenced the transcriptomes of *EBF1*-overexpressing cells. Using the Genomic Regions Enrichment of Annotations Tool (GREAT) algorithm (42), we found that genes downregulated by *EBF1* overexpression were enriched in pathways related to chromosomal organization, reassuringly including *TERT* (Supplemental Figure 3D, left). Reciprocally, we found that genes upregulated by *EBF1* overexpression, including *FAS*, *HIF1A*, and *AIFM2*, were enriched in pathways such as cell death regulation (Supplemental Figure 3D, right).

EBF1 exhibits dominant-negative mutations in GC. To obtain further evidence of *EBF1* disruptions in GC, we investigated whether *EBF1* exhibits somatic DNA mutations that might alter *EBF1* function. We queried exome- and whole-genome sequencing data for 459 GCs from public and in-house data sets and iden-

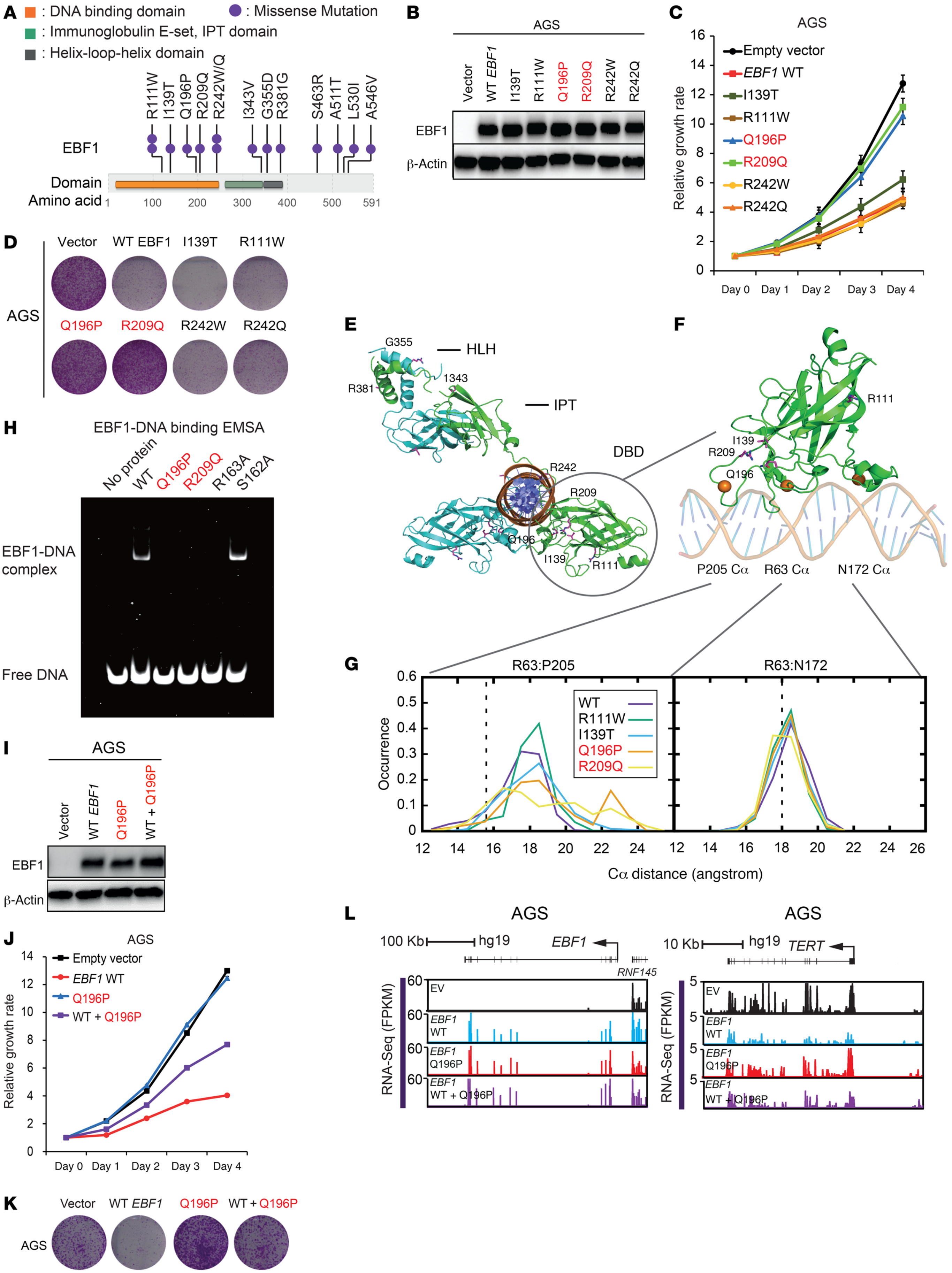
A
: DNA binding domain
: Missense Mutation
: Immunoglobulin E-set, IPT domain
: Helix-loop-helix domain
R111W
I139T
Q196P
R209Q
R242W/Q
I343V
G355D
R381G
S463R
A511T
L530I
A546V
EBF1
Domain
Amino acid
1
100
200
300
400
500
591
B
AGS
Vector
WT EBF1
I139T
R111W
Q196P
R209Q
R242W
R242Q
EBF1
β-Actin
C
AGS
Relative growth rate
Empty vector
EBF1 WT
I139T
R111W
Q196P
R209Q
R242W
R242Q
Day 0
Day 1
Day 2
Day 3
Day 4
D
AGS
Vector
WT EBF1
I139T
R111W
Q196P
R209Q
R242W
R242Q
E
G355
HLH
R381
1343
IPT
DBD
R242
R209
Q196
I139
R111
F
R111
I139
R209
Q196
P205 Cα
R63 Cα
N172 Cα
G
R63:P205
R63:N172
Occurrence
WT
R111W
I139T
Q196P
R209Q
Cα distance (angstrom)
H
EBF1-DNA binding EMSA
No protein
WT
Q196P
R209Q
R163A
S162A
EBF1-DNA complex
Free DNA
I
AGS
Vector
WT EBF1
Q196P
WT + Q196P
EBF1
β-Actin
J
AGS
Relative growth rate
Empty vector
EBF1 WT
Q196P
WT + Q196P
Day 0
Day 1
Day 2
Day 3
Day 4
K
Vector
WT EBF1
Q196P
WT + Q196P
AGS
L
AGS
100 Kb
hg19
EBF1
RNF145
RNA-Seq (FPKM)
EV
EBF1 WT
EBF1 Q196P
EBF1 WT + Q196P
AGS
10 Kb
hg19
TERT
RNA-Seq (FPKM)
EV
EBF1 WT
EBF1 Q196P
EBF1 WT + Q196P

Figure 4. *EBF1* exhibits dominant-negative somatic mutations in GC. (**A**) Distribution of *EBF1* coding mutations in 14 GC patients with annotated functional domains. Each dot represents 1 patient. (**B**) Western blotting revealed equal levels of EBF1 protein abundance after overexpression of WT and mutant EBF1 in AGS cells. (**C** and **D**) Proliferation assays (**C**) and monolayer colony formation assays (**D**) showed cell proliferation capacity after overexpression of WT and mutant *EBF1* in GC cells. Error bars indicate SD. (**E**) 3D structural analysis of EBF1 and missense mutations. The x-ray crystal structure reveals that 2 EBF1 protomers (green and cyan ribbons) are predicted to dimerize and bind to DNA (orange ribbon with blue ladders). Purple sticks and labels indicate the positions of GC-associated missense mutations on 3 functional domains. HLH, helix-loop-helix. (**F** and **G**) Alterations of DNA-binding loop flexibility by *EBF1* mutations. (**F**) EBF1 DBDs are represented by green ribbons. Purple sticks indicate the position of 4 missense mutations. The 3 orange beads mark Cα atoms of R63, N172, and P205. Double helix shows the relative orientation of DNA in the complex. (**G**) Distance distributions of specified Cα atoms obtained from MD simulations of unbound EBF1 DBD. Vertical dashed lines indicate the distances measured from x-ray crystal structures. (**H**) EMSAs showed that Q196P or R209Q mutated recombinant EBF1 protein did not have DNA binding to probes containing EBF1-binding motifs. (**I**) Western blots showed similar protein levels of WT EBF1, Q196P-mutant EBF1, and combined WT plus Q196P-mutant EBF1 after overexpression. Proliferation assay (**J**) and monolayer colony formation assay (**K**) showed cell proliferation capacity after overexpression. Error bars indicate SD. (**L**) Gene expression levels (RNA-Seq) of AGS cells after retroviral infection with either empty vector (black), WT *EBF1* (blue), Q196P-mutant *EBF1* (red), or combined WT plus Q196P-mutant *EBF1* (purple). Expression levels of *EBF1* and *TERT* are shown.

tified 14 GCs with *EBF1* coding missense mutations (Figure 4A). Of these, 50% of the mutations were localized to the *EBF1* DNA–binding domain (DBD), targeting highly conserved sequence residues (Supplemental Figure 4A). To distinguish passenger from driver mutations, we individually cloned the *EBF1* DBD mutations and expressed the *EBF1* mutants in 2 GC cell lines that normally do not express *EBF1* (AGS and SNU484). In both cell lines, Western blotting confirmed comparable expression levels of both WT and mutant EBF1 proteins (Figure 4B and Supplemental Figure 4B). Proliferation and monolayer colony formation assays showed that WT *EBF1* dramatically reduced cellular proliferation and monolayer colony formation (Figure 4, C and D, and Supplemental Figure 4, C and D). In contrast, the *EBF1* mutants Q196P and R209Q had a proliferative capacity similar to that of empty vector controls, demonstrating that Q196P and R209Q mutations are sufficient to abolish *EBF1* activity. I139T, R111W, and R242W/Q mutants exhibited a proliferative capacity similar to that of WT *EBF1* and were designated passengers.

To investigate the structural impact of Q196P and R209Q mutations on EBF1 activity, we performed 3D structural analysis and molecular dynamic (MD) simulations. Mapping of the Q196P and R209Q mutations to *EBF1*-DNA complex structures revealed that these residues are probably not directly involved in DNA contact or DNA recognition (Figure 4, E and F). Using MD simulations to investigate the effect of these mutations at the atomic level, we determined that both WT and mutant EBF1 DBDs are predicted to exhibit similar integrity and stability under both unbound and DNA-bound states (Supplemental Figure 4, E and F). However, during the unbound EBF1 simulations, the Q196P and R209Q mutants showed loss of intramolecular hydrogen bonds in the DBD GH loop (aa 193–210), which would be predicted to cause greater loop flexibility and a longer time to attain a proper DNA-binding conformation (Figure 4G). Also, compared with the WT *EBF1* DBD, we found that the Q196P and R209Q mutants had energetically less favorable associations with DNA (Supplemental Table 2). These results suggest that Q196P and R209Q *EBF1* DBDs are likely to bind less stably to DNA compared with WT *EBF1*. To confirm this prediction, we performed EMSAs using recombinant EBF1 proteins. Compared with WT EBF1, Q196P- or R209Q-mutated EBF1 did not display DNA binding to probes containing EBF1-binding motifs (Figure 4H).

The *EBF1* mutations observed in GC were heterozygous, indicating that *EBF1*-mutated GCs may still express a WT copy of *EBF1*. However, *EBF1* has been shown to function as a dimer (43), raising the possibility that the Q196P and R209Q mutations may function as dominant-negative isoforms. To test this possibility, we induced co-overexpression of WT and Q196P *EBF1* in AGS cells. We found that cells coexpressing WT and Q196P *EBF1* had compromised proliferation rates, decreased monolayer colony formation, and reduced *TERT* mRNA levels, intermediate between *EBF1* WT and Q196P-mutant cells (Figure 4, I–L, and Supplemental Figure 4G). These results suggest that certain *EBF1* DBD mutations have dominant-negative activity.

EBF1 binds to a TERT 5′ proximal cis-regulatory element. To determine whether EBF1 occupies *cis*-regulatory elements at the *TERT* promoter, we performed EBF1 ChIP-Seq in *EBF1*-expressing GC cell lines (HGC27, Hs746T, YCC11, and AGS with endogenous *EBF1*). We also analyzed AGS cells overexpressing either WT *EBF1* or the *EBF1* DNA–binding mutants. Motif analysis of the *EBF1* ChIP-Seq peaks revealed that the top-ranked de novo consensus binding motif matched previously known *EBF1* factors (Figure 5A and refs. 44, 45). We identified 2 *EBF1*-binding peaks in the *TERT* 5′ proximal region, at –2.3 kb and –4 kb, both with EBF1-binding motifs (hereafter referred to as peak 1 and peak 2, respectively) (Figure 5B). We observed no EBF1 binding at peaks 1 or 2 in cell lines lacking endogenous *EBF1* or in cells overexpressing mutant *EBF1* (Q196P or R209Q), further demonstrating that certain *EBF1* DBD mutations have decreased DNA-binding capacity (Figure 5B). Besides peak 1 and peak 2 at the *TERT* 5′ proximal region, expanded analysis of the *TERT* genomic locus did not reveal significant or consistent EBF1 binding at other distal regions, suggesting that peaks 1 and 2 are the predominant EBF1-binding regions at *TERT* in GC (Supplemental Figure 5A).

To determine whether the *TERT* 5′ proximal region containing peaks 1 and 2 has properties of an enhancer element, we then mapped potential *cis*-regulatory elements and chromatin features associated with the *TERT* 5′ proximal region using Nano-ChIP-Seq histone profiles (46). Specifically, we compared GC cell lines expressing high and low *TERT* transcription levels and also primary GCs relative to matched normal tissues (Figure 5C and sequencing statistics in Supplemental Table 3). Concentrating on H3K27ac and H3K4me1 modifications corresponding to activity and enhancer marks, respectively (47), we reidentified a previously described *TERT*-regulatory element 21 kb upstream of the *TERT* TSS, supporting the reliability of our data (Figure 5C, gray bar, and ref. 48). Notably, we observed increased H3K27ac and H3K4me1 signals at peak 2 in primary GCs compared with matched normal

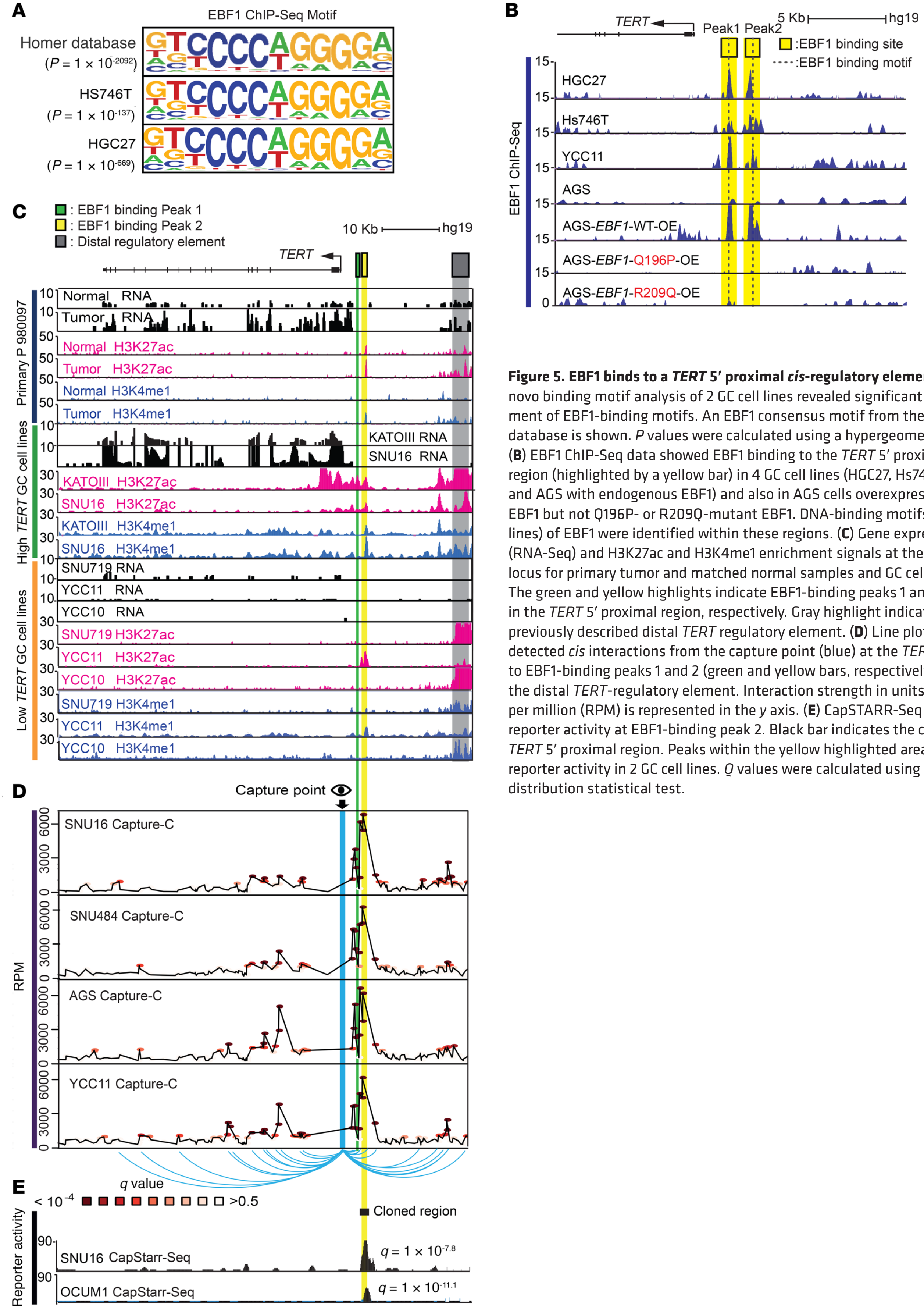

Figure 5. EBF1 binds to a *TERT* 5′ proximal *cis*-regulatory element. (**A**) De novo binding motif analysis of 2 GC cell lines revealed significant enrichment of EBF1-binding motifs. An EBF1 consensus motif from the HOMER database is shown. *P* values were calculated using a hypergeometric test. (**B**) EBF1 ChIP-Seq data showed EBF1 binding to the *TERT* 5′ proximal region (highlighted by a yellow bar) in 4 GC cell lines (HGC27, Hs746T, YCC11, and AGS with endogenous EBF1) and also in AGS cells overexpressing WT EBF1 but not Q196P- or R209Q-mutant EBF1. DNA-binding motifs (dashed lines) of EBF1 were identified within these regions. (**C**) Gene expression (RNA-Seq) and H3K27ac and H3K4me1 enrichment signals at the *TERT* locus for primary tumor and matched normal samples and GC cell lines. The green and yellow highlights indicate EBF1-binding peaks 1 and 2 in the *TERT* 5′ proximal region, respectively. Gray highlight indicates a previously described distal *TERT* regulatory element. (**D**) Line plots show detected *cis* interactions from the capture point (blue) at the *TERT* TSS to EBF1-binding peaks 1 and 2 (green and yellow bars, respectively) and the distal *TERT*-regulatory element. Interaction strength in units of reads per million (RPM) is represented in the *y* axis. (**E**) CapSTARR-Seq showed reporter activity at EBF1-binding peak 2. Black bar indicates the cloned *TERT* 5′ proximal region. Peaks within the yellow highlighted area indicate reporter activity in 2 GC cell lines. *Q* values were calculated using a Poisson distribution statistical test.

tissue (Figure 5C, yellow bar) and also in cell lines with high *TERT* expression (KATO III and SNU16) compared with cell lines with low *TERT* expression (SNU719, YCC11, and YCC10). H3K27ac signals were also observed at peak 1 in the *TERT*-expressing lines KATO III and SNU16. To determine whether chromatin accessibility at the *TERT* locus correlates with *TERT* transcription, we performed ATAC-Seq on 6 GC cell lines with high or low *TERT* expression. We observed higher levels of chromatin accessibility across the *TERT* locus (including the 5′ proximal region containing peaks 1 and 2) in cell lines with high *TERT* expression (Supplemental Figure 5B, blue bar) and lower levels of chromatin accessibility in cell lines with low *TERT* expression. To assess whether DNA modifications, such as 5-methylcytosine (5mC) and 5-hydroxymethyl (5hmC), also correlate with *TERT* expression, we next performed 5mC and 5hmC profiling on cell lines with high or low TERT expression. However, we did not observe 5mC or 5hmC signals in this proximal element with *EBF1*-binding peaks, in cell lines with either high or low *TERT* expression (Supplemental Figure 5D and see Discussion). It is possible that *TERT* expression in GC is uncorrelated with DNA methylation levels or, alternatively, that because *TERT* is a low-expression gene (49), changes in *TERT* DNA methylation were below the limits of detection of the 5mc and 5hmc profiling methods used in this study.

We asked whether the *TERT* TSS might interact with the peak 1 and 2 regions via chromatin interactions (50). Applying Capture-C technology on 4 GC cell lines (AGS, SNU16, SNU484, and YCC11) targeting the *TERT* TSS, we confirmed that both peaks 1 and 2 had chromatin interactions with the *TERT* TSS (Figure 5D and see Methods). However, despite occurring more distal to the *TERT* TSS, peak 2 showed stronger TSS interactions compared with peak 1. This suggests that although both peaks 1 and 2 may contribute to *TERT* regulation, peak 2 may play a stronger role, consistent with peak 2 having stronger epigenomic signals of enhancers (Figure 5C). To determine whether peak 2 had properties of a functional enhancer, we also applied CapSTARR-Seq technology, a high-throughput technique for functional testing of candidate enhancer elements (see Methods). Using this approach, peak 2 was confirmed to have enhancer activity (SNU16, $Q = 1.58 \times 10^{-8}$; OCUM1, $Q = 7.9 \times 10^{-12}$; Figure 5E). Interestingly, although YCC11 is a cell line expressing low levels of *TERT*, we observed similar levels of *cis* interactions compared with cell lines expressing high levels of *TERT* (SNU16, SNU484, and AGS), supporting recent studies showing that many *cis* interactions are largely stable and preformed (51, 52). To explore global chromatin interaction landscapes in the *TERT* locus, we also performed Hi-C chromatin conformation profiling in cell lines with high (SNU16) and low (SNU719) *TERT* expression. Hi-C interactions at the *TERT* locus were higher in SNU16 cells than in SNU719 cells (Supplemental Figure 5C).

Genomic alterations of the TERT 5′ proximal region in primacy GC. In other cancers, large-scale genomic alterations at the *TERT* locus (e.g., translocations, copy number variants) have been shown to deregulate *TERT* expression (19, 20). To investigate whether the *TERT* 5′ proximal region containing peaks 1 and 2 might be associated with genomic alterations in vivo, we examined structural variants (SVs) at the *TERT* locus in 212 primary GCs and 62 cell lines (25). We identified 2 GCs (P990489 and HK-PFG144T) and 1 GC cell line (LMSU) that had somatic deletions or rearrangements affecting the *TERT* 5′ proximal region including peaks 1 and 2 (Figure 6). In GC P990489, the deletion was a highly focal 1-kb deletion, occurring at –3.5 to –4.4 kb, coinciding with peak 2 (Figure 6A), whereas LMSU cells harbored a genomic rearrangement deleting both peak 1 and peak 2 (Figure 6B). For both GC P990489 and LMSU cells, the 5′ *TERT* alterations were orthogonally confirmed by Sanger sequencing (Figure 6, C and D). At the expression level, GC P990489, harboring a deletion of the *TERT* 5′ proximal region, had the second-highest level of *TERT* overexpression in our in-house cohort (>8 fold higher compared with matched normal samples) (Figure 6E), and LMSU GC cells had high *TERT* mRNA expression, ranking 11th in our in-house panel of 63 gastric cell lines (Supplemental Figure 1B). We also performed telomere length measurements and observed an increase in GC P990489 telomere lengths compared with those of matched normal tissue (Figure 6F). The third GC (HK-PFG144T) also harbored a deletion affecting both peaks (Supplemental Figure 6A). These results suggest that in certain GCs, the *TERT* 5′ proximal region containing peaks 1 and 2 is associated with genomic deletions and/or rearrangements, which are predicted to delete and rearrange EBF1-binding sites.

To functionally test the role of peak 1 and peak 2 in *TERT* regulation, we performed CRISPR-mediated genomic deletion of both peaks 1 and 2 in a GC cell line (YCC11) expressing low levels of *TERT*. Data from multiple single-cell clones, with homozygous deletion of both *TERT* regions, consistently showed upregulated *TERT* expression compared with intact clones ($P < 0.05$; Figure 6G). We further introduced CRISPR-mediated point mutations to disrupt the EBF1-binding motifs of both regions in YCC11 cells (see Methods). After sequence verification (Supplemental Figure 6B), we analyzed single-cell clones with mutations in at least 1 allele in either or both of the peak 1 and peak 2 EBF1-binding motifs (i.e., peak 1, heterozygous; peak 2, heterozygous; peaks 1 and 2, heterozygous; peak 2, homozygous). Using qPCR to access *TERT* expression, we detected higher *TERT* expression levels across all the mutated clones compared with levels in WT clones ($P < 0.05$; Figure 6H). These results suggest that both peaks probably contribute to *TERT* regulation.

To determine whether the *TERT* 5′ proximal region is also associated with genomic alterations in other cancers, we surveyed published studies across 32 cancer types (19, 53) and identified 10 more cases with genomic rearrangements affecting the *TERT* 5′ proximal region. These included 2 chromophobe renal cell carcinomas (KICH, TCGA), 1 urothelial bladder cancer (BLCA, TCGA), 2 sarcomas (SARC, TCGA), 2 hepatocellular carcinomas (LIHC, TCGA), and 3 neuroblastomas (NBL) (Figure 6I), suggesting that the *TERT* 5′ proximal region is associated with genomic alterations in other cancer types besides GC. Notably, in a total of 13 cases, genomic alterations affected both peaks 1 and 2 in 11 cases and peak 2 in 2 cases, indicating the importance of both peaks in contributing to *TERT* regulation.

Discussion

TERT overexpression is a signature hallmark of cancer. In GC, Gigek et al. reported that *TERT* expression was detected in 80%

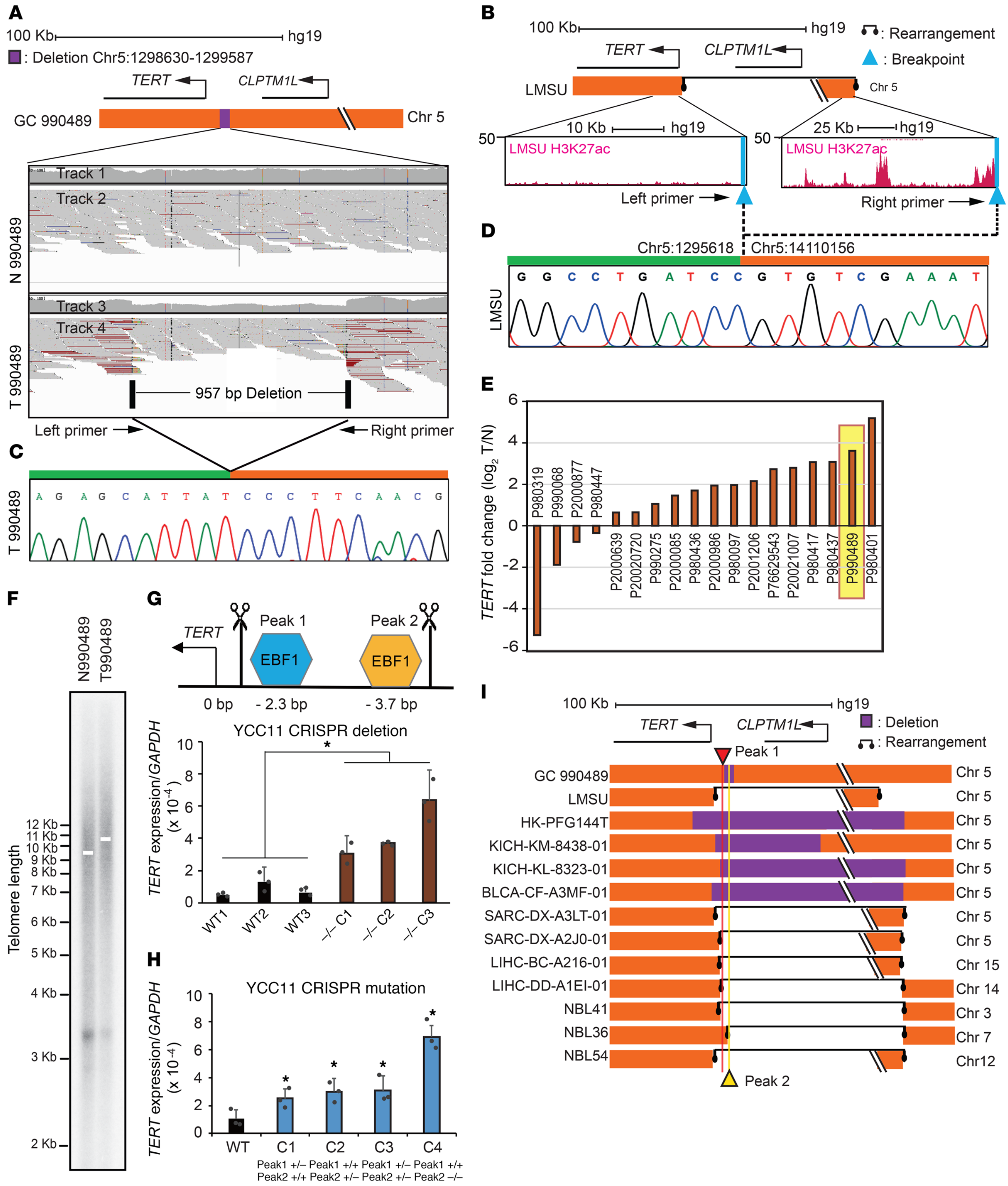
A
100 Kb
hg19
■ : Deletion Chr5:1298630-1299587
TERT
CLPTM1L
GC 990489
Chr 5
Track 1
Track 2
N 990489
Track 3
Track 4
T 990489
957 bp Deletion
Left primer
Right primer
C
T 990489
A G A G C A T T A T C C C T T C A A C G
B
100 Kb
hg19
: Rearrangement
: Breakpoint
TERT
CLPTM1L
LMSU
Chr 5
10 Kb
hg19
50
LMSU H3K27ac
25 Kb
hg19
50
LMSU H3K27ac
Left primer
Right primer
D
Chr5:1295618
Chr5:14110156
LMSU
G G C C T G A T C C G T G T C G A A A T
E
TERT fold change (log2 T/N)
6
4
2
0
-2
-4
-6
P980319
P990068
P2000877
P980447
P2000639
P20020720
P990275
P2000085
P980436
P2000986
P980097
P2001206
P76629543
P20021007
P980417
P980437
P990489
P980401
F
N990489
T990489
Telomere length
12 Kb
11 Kb
10 Kb
9 Kb
8 Kb
7 Kb
6 Kb
5 Kb
4 Kb
3 Kb
2 Kb
G
TERT
Peak 1
Peak 2
EBF1
EBF1
0 bp
- 2.3 bp
- 3.7 bp
YCC11 CRISPR deletion
TERT expression/GAPDH (x 10-4)
10
8
6
4
2
0
*
WT1
WT2
WT3
-/- C1
-/- C2
-/- C3
H
YCC11 CRISPR mutation
TERT expression/GAPDH (x 10-4)
10
8
6
4
2
0
*
*
*
*
WT
C1
C2
C3
C4
Peak1 +/– Peak1 +/+ Peak1 +/– Peak1 +/+
Peak2 +/+ Peak2 +/– Peak2 +/– Peak2 –/–
I
100 Kb
hg19
TERT
CLPTM1L
■ : Deletion
: Rearrangement
Peak 1
GC 990489
LMSU
HK-PFG144T
KICH-KM-8438-01
KICH-KL-8323-01
BLCA-CF-A3MF-01
SARC-DX-A3LT-01
SARC-DX-A2J0-01
LIHC-BC-A216-01
LIHC-DD-A1EI-01
NBL41
NBL36
NBL54
Chr 5
Chr 5
Chr 5
Chr 5
Chr 5
Chr 5
Chr 5
Chr 5
Chr 15
Chr 14
Chr 3
Chr 7
Chr12
Peak 2

Figure 6. Genomic alterations of the *TERT* 5′ proximal region in primacy GC. (**A**) Somatic large-scale genomic deletion affecting EBF1-binding peak 2 in GC T990489. Tracks 1 and 3: aligned read coverage from WGS profiles. Tracks 2 and 4: distribution of aligned reads. Red reads in track 4 have larger-than-expected inferred sizes and therefore indicate possible deletions. Lower coverage in track 3 with respect to track 1 at the same loci supports the existence of a somatic genomic deletion. Purple box indicates the genomic deleted region. (**B**) Translocation disrupting the *TERT* 5′ proximal region (including both EBF1-binding peaks 1 and 2) in LMSU cells. Blue bars indicate breakpoints of the translocation. Dark pink tracks depict H3K27ac signals. (**C** and **D**) Validation of somatic genomic deletion/translocation of the *TERT* 5′ proximal region in GC T990489 and LMSU lines via Sanger sequencing. (**E**) Log-transformed fold change of *TERT* expression in 18 GCs with respect to matched normal samples. GC P990489 is highlighted in yellow. (**F**) Telomere lengthening was observed in GC T990489 by Southern blotting and densitometric analysis. (**G**) The CRISPR-deleted region is indicated by scissors (top). Graph shows a comparison of *TERT* expression between WT YCC11 clones (black bars) and clones (C1, C2, C3) with CRISPR-mediated homozygous deletions at the *TERT* 5′ proximal region (brown bars). (**H**) Comparison of *TERT* expression between WT clones (black) and clones with mutations in at least 1 allele in 1 or both EBF1-binding motifs (blue). (**I**) Deletions/translocations that overlapped with the *TERT* 5′ proximal region are shown for 2 GC cases, 1 GC cell line, and 10 cases of other cancer types. Vertical red and yellow lines highlight EBF1-binding peaks 1 and 2. $^*Q < 0.05$, by 2-sided t test with FDR multiple testing correction (**G** and **H**). RT-PCR results are shown as the mean ± SD of technical triplicates. Figures are representative of 3 independent experiments.

of gastric tumors but not in normal gastric mucosa (24), and other studies have also reported significant *TERT* overexpression in GC (22, 23). In this study, we performed a comprehensive analysis of *TERT* expression in GC. We queried RNA-Seq data from TCGA cohort and confirmed that *TERT* was significantly overexpressed in GC and that all 4 GC molecular subtypes exhibited significantly higher *TERT* expression levels than those in normal samples. We further replicated these findings in an independent RNA-Seq data set of 18 T/N pairs. Studies in different tumor types have highlighted distinct mechanisms for *TERT* transcriptional reactivation. At the *cis*-regulatory level, *TERT* promoter mutations at C250T and C228T have been primarily observed in glioblastoma (89%), melanoma (72%), and bladder cancer (70%) (16, 17), creating de novo binding motifs for ETS TFs and activating *TERT* (41). In other tumor types such as neuroblastoma, lung cancer, colon cancer, and cervical cancer, studies have reported large-scale SVs and copy number alterations involving *TERT* that can also cause high expression of *TERT* by affecting noncoding regulatory elements at the *TERT* locus (19, 20). However, specific mechanisms underlying *TERT* reactivation in GC remain largely unknown. In this study, we identified the TF *EBF1* as a direct repressor of *TERT* expression. Our results also suggest that in GC, *TERT* is reactivated by abolishing *EBF1* function via at least 3 distinct mechanisms: (a) epigenetic silencing of *EBF1* expression via PRC2, DNA methyltransferase, and HDAC activity; (b) somatic *EBF1* mutations resulting in dominant-negative isoforms; and (c) deletion or rearrangement of *EBF1*-binding sites proximal to the *TERT* promoter.

The discovery of *EBF1* as a *TERT* repressor is notable. To date, 4 EBF family TFs have been described (*EBF1*, *EBF2*, *EBF3*, and *EBF4*) and shown to play important developmental roles in the regulation of cell fate decisions, differentiation, and migration (54). Besides B cell development (55), *EBF1* has been reported to regulate adipocyte differentiation and morphology (56, 57) and also the differentiation of sensory neurons (58), highlighting a role for *EBF1* beyond the hematopoietic system. Supporting these findings, in vivo studies of *EBF1* in *Ebf1*$^{+/-}$ mice on a high-fat diet revealed white adipose tissue (WAT) hypertrophy and insulin resistance (57). In addition, late *Ebf1*$^{-/-}$ embryos were shown to have specific increases in striatal cell death and reductions in size after birth (58). In cancer, *EBF1* has been proposed as a potential tumor suppressor (28) in malignancies such as breast cancer, in which *EBF1* genomic deletions have been reported in 18.9% of breast cancer lines (29). *EBF1* has also been proposed as an important epigenetic modifier in breast cancer (59), and in cholangiocarcinoma (CCA), *EBF1* downregulation through prolonged oxidative stress was reported to induce tumorigenic properties (60). Interestingly, besides GC, analysis of RNA-Seq data across other TCGA cancer types revealed similar negative correlations between *EBF1* and *TERT* (Supplemental Figure 6C). *EBF1* may thus regulate *TERT* in other cancer types, although this hypothesis will require further investigation.

Our data suggest that in GC, *EBF1* is downregulated in primary tumors particularly through epigenetic silencing. Specifically, at the level of DNA promoter hypermethylation, approximately half (40%–55%) of primary GCs with loss of *EBF1* expression exhibited high levels of *EBF1* promoter methylation.

Besides being silenced by epigenetic regulation, *EBF1* was also found to exhibit somatic mutations resulting in dominant-negative isoforms. We observed *EBF1* somatic point mutations in 3.1% of GCs, half of which occurred within the highly conserved *EBF1* DBD. Functional experiments support the notion that some of these mutations (e.g., Q196P) strongly abrogate the ability of *EBF1* to inhibit cell proliferation. Notably, although these *EBF1* mutations were heterozygous, we found that they had dominant-negative activity, which is likely explained by the fact that EBF1 protein acts as a dimer (43). In the literature, other examples of "single-hit" tumor suppressors include *FBXW7* (61) and *p53* (62), which also result in the creation of dominant-negative isoforms. We also note that the presence of functional somatic *EBF1* mutations in GC provides further support for *EBF1* activity in the stomach.

A third and distinct mechanism of abrogation of EBF1 function occurred through deletions and rearrangements of *EBF1*-binding sites proximal to the *TERT* promoter. Specifically, we identified a regulatory element close to the *TERT* promoter that interacts with the *TERT* TSS, containing EBF1-binding sites and demonstrating EBF1 occupancy. CRISPR-mediated deletion of this region, or CRISPR-induced mutations of EBF1-binding motifs in either or both peaks, resulted in increased *TERT* expression in GCs expressing low levels of *TERT*. Epigenomic analysis revealed that this region was silenced in GCs with low *TERT* expression and active in GCs with high *TERT* expression, raising the possibility that this *TERT* 5′ proximal region may function as a regulatory "rheostat," recruiting transcriptional repressors or activators in GCs expressing low and high levels of *TERT*, respectively. Importantly, this region exhibited somatic deletions and rearrangements in certain GCs and other tumor types, confirming its disruption in vivo. Interestingly, for LMSU cells, analysis of in-house H3K27ac ChIP-Seq data on GC cell lines suggested that, besides deleting this

TERT 5′ proximal region, genomic rearrangements in these cells may also cause genomic fusion of the 5′ *TERT* region with 2 distal superenhancers (Figure 6B). Genomic disruptions of this region may be required for high *TERT* expression, as the *TERT* upstream region is well known to show strong epigenetic repression across multiple cell types (63).

In conclusion, telomerase has attracted interest as a target for cancer therapy, as most somatic cells have no or only low-level telomerase activity, whereas up to 90% of human cancers have transcriptionally reactivated *TERT*. Numerous telomerase-based therapeutic strategies are under investigation, such as the telomerase inhibitor imetelstat (GRN163L) and telomerase-derived anticancer peptide vaccines (GV1001 and GRNVAC1) (64). However, recent clinical trial results for GRN163L have shown significant dose-dependent hematological side effects, liver function abnormalities, and other adverse effects (65), which may be due to simultaneous inhibition of telomerase activity in both cancer cells and normal tissue–specific stem/progenitor cells. Thus, there remains an urgent need to elucidate the basic mechanisms of telomerase reactivation in cancer, which may highlight new strategies to inhibit telomerase. In particular, combinatorial inhibition of epigenetic pathways regulating *EBF1* expression may prove to be an interesting area for further study.

Methods

Cell lines. AGS, KATO III, SNU16, and Hs746T cells were obtained from the American Type Culture Collection (ATCC). SNU719 and SNU484 cells were obtained from the Korean Cell Line Bank (KCLB). LMSU, GSS, and HGC27 cells were obtained from the RIKEN cell bank. IM95 cells were obtained from the Japanese Collection of Research Bioresources (JCRB) Cell Bank. YCC10 and YCC11 cells were gifts from Yonsei Cancer Centre (Seoul, South Korea). Cell line identities were confirmed by short tandem repeat (STR) DNA profiling performed at the Centre for Translational Research and Diagnostics (Cancer Science Institute of Singapore, Singapore), and STR profiles were assessed according to the standard American National Standards Institute/ATCC (ANSI/ATCC) ASN-0002-2011 nomenclature. The profiles of cell lines showed greater than 80% similarity to reference databases. All cell lines were negative for mycoplasma contamination.

Statistics. For Capture-C data analysis, r3Cseq was used to identify significant interactions of the viewpoint against a scaled background ($Q < 0.05$). For CapSTARR-Seq data analysis, an enhancer peak was called when there was significant enrichment of fragments from 1 region in the output library compared with the representation of that region in the input library based on Poisson distribution using MACS2 (https://github.com/taoliu/MACS/). Histone ChIP-enriched peaks were detected using the control-based ChIP-Seq analysis tool CCAT (https://github.com/vanbug/cluster/tree/master/cluster/CCAT/CCAT3.0) (FDR <5%). TF ChIP-enriched peaks were detected using MACS2 with the following thresholds: $Q < 0.05$ for paired-end sequencing and $P < 0.00005$ for single-end sequencing. TF-binding motifs were predicted using detected TF-binding sites from ChIP-Seq and HOMER (Hypergeometric Optimization of Motif EnRichment; http://homer.ucsd.edu/homer/motif/) with default parameters. For the immunohistochemistry studies in Supplemental Table 1, a Mann-Whitney U test was used for comparisons between 2 groups, whereas a Kruskal-Wallis test was used for comparisons of more than 2 groups. For cell phenotype assays, tumor xenograft studies, qPCR assays, real-time TRAP assays, and immunohistochemical analyses, P values were calculated using a 2-sided t test. A P value of less than 0.05 was considered statistically significant. FDR-based multiple testing correction was applied for multiple comparisons when applicable. A Q value of less than 0.05 was considered statistically significant. For comparison of gene expression levels between tumor samples and normal samples in Figure 1A, a Wilcoxon's rank-sum test with multiple testing correction using the FDR procedure was performed against normal expression levels. For comparison of gene expression levels between all tumor samples and normal samples in Figure 1H and Supplemental Figure 1A, a Wilcoxon's rank-sum test was performed against normal expression levels. For the correlation analysis in Figure 1C and Supplemental Figure 6C, P values for correlation were calculated using Pearson's correlation test. For correlation analysis in Figure 1B and Figure 2A, P values for correlation were calculated using Pearson's correlation test with multiple testing correction with the FDR procedure.

Histone ChIP-Seq, TF ChIP-Seq, Capture-C, CapSTARR-Seq, and RNA-Seq data sets are available in the Gene Expression Omnibus (GEO) database (GEO GSE121140). The public data sets used are described in the Supplemental Methods.

Study approval. Patients' primary samples were obtained from the SingHealth tissue repository with approval from the SingHealth Centralised IRB and signed patient informed consent. Animal studies were conducted in compliance with animal protocols approved by the SingHealth IACUC of Singapore. Additional details, including the methods associated with WGS and structural variant detection, ChIP-Seq, RNA-Seq, telomere length measurements, Capture-C, CRISPR/Cas9, silencing and overexpression of *EBF1*, tumor xenografts, DNA methylation analysis, real-time TRAP assays, drug treatments, CapSTARR-Seq, MD simulations, MethylLight assays, ATAC-Seq, EMSAs, detection of *EBF1* coding mutations, EBF1 immunohistochemistry, Western blotting, Sanger sequencing, cell phenotype assays, qPCR, and data availability are described in the Supplemental Methods.

Author contributions

MX, WFO, JT, SL, BTT, and PT conceptualized the study. MX, WFO, JT, AQ, PHL, CX, NP, JQL, XY, MA, LMN, TS, CGAN, MR, LM, TN, TY, KD, JSL, KW, SGR, MB, RSYF, HIG, AJS, SL, and PT developed methodology. MX, WFO, AQ, PHL, JQL, YAG, KKH, SWTH, KJL, TN, MMC, JSL, and AJS analyzed data. MX, JT, ZL, JW, MR, LM, GF, GCW, SZ, TY, KD, ZFAI, JW, PPSY, YNL, STT, ML, ALKT, and XO performed experiments. MX and PT wrote the manuscript. PT supervised the study.

Acknowledgments

We thank Yoshiaki Ito and Shing Leng Chan for helpful discussions. We thank Angie Tan, Beatrice Tan, and Hui Hoon Chua for their administrative support. We also thank members of the Duke-NUS Genome Biology Facility and the Sequencing and Scientific Computing teams at the Genome Institute of Singapore for providing sequencing services and data management capabilities. This work was supported by National Medical Research Council grants TCR/009-NUHS/2013, OFLCG18May-0003, NMRC/STaR/0026/2015, and OFIRG15nov072; National University Cancer Institute, Singapore (NCIS) grant NR13NMR111OM;

A*STAR A*ccelerate GAP grant ETPL/15-R15 GAP-0021; Ministry of Education Academic Research Tier 2 grant MOE2017-T2-1-105; Guangdong Innovative and Entrepreneurial Research Team Program grants 2016ZT06S638 and 2016ZT06S252; and National Natural Science Foundation of China grant 61661146004. Funding was also provided by the Cancer Science Institute of Singapore, NUS, under the National Research Foundation Singapore and the Singapore Ministry of Education under its Research Centres of Excellence initiative, and block funding was received from Duke-NUS Medical School.

Address correspondence to: Patrick Tan, Duke-NUS Medical School, 8 College Road #07-19, Singapore 169857. Phone: 65.6516.1783; Email: gmstanp@duke-nus.edu.sg.

---

1. Ferlay J, et al. Cancer incidence and mortality worldwide: sources, methods and major patterns in GLOBOCAN 2012. *Int J Cancer*. 2015;136(5):E359–E386.
2. Seyedin S, Wang PC, Zhang Q, Lee P. Benefit of adjuvant chemoradiotherapy for gastric adenocarcinoma: a SEER population analysis. *Gastrointest Cancer Res*. 2014;7(3-4):82–90.
3. Bang YJ, et al. Trastuzumab in combination with chemotherapy versus chemotherapy alone for treatment of HER2-positive advanced gastric or gastro-oesophageal junction cancer (ToGA): a phase 3, open-label, randomised controlled trial. *Lancet*. 2010;376(9742):687–697.
4. Fuchs CS, et al. Ramucirumab monotherapy for previously treated advanced gastric or gastro-oesophageal junction adenocarcinoma (REGARD): an international, randomised, multicentre, placebo-controlled, phase 3 trial. *Lancet*. 2014;383(9911):31–39.
5. Schnipper LE, et al. American Society of Clinical Oncology statement: a conceptual framework to assess the value of cancer treatment options. *J Clin Oncol*. 2015;33(23):2563–2577.
6. Kang YK, et al. Nivolumab in patients with advanced gastric or gastro-oesophageal junction cancer refractory to, or intolerant of, at least two previous chemotherapy regimens (ONO-4538-12, ATTRACTION-2): a randomised, double-blind, placebo-controlled, phase 3 trial. *Lancet*. 2017;390(10111):2461–2471.
7. Waddell T, et al. Epirubicin, oxaliplatin, and capecitabine with or without panitumumab for patients with previously untreated advanced oesophagogastric cancer (REAL3): a randomised, open-label phase 3 trial. *Lancet Oncol*. 2013;14(6):481–489.
8. Lordick F, et al. Capecitabine and cisplatin with or without cetuximab for patients with previously untreated advanced gastric cancer (EXPAND): a randomised, open-label phase 3 trial. *Lancet Oncol*. 2013;14(6):490–499.
9. Satoh T, et al. Lapatinib plus paclitaxel versus paclitaxel alone in the second-line treatment of HER2-amplified advanced gastric cancer in Asian populations: TyTAN--a randomized, phase III study. *J Clin Oncol*. 2014;32(19):2039–2049.
10. Lordick F, Lorenzen S, Yamada Y, Ilson D. Optimal chemotherapy for advanced gastric cancer: is there a global consensus? *Gastric Cancer*. 2014;17(2):213–225.
11. Shay JW, Bacchetti S. A survey of telomerase activity in human cancer. *Eur J Cancer*. 1997;33(5):787–791.
12. Shay JW, Wright WE. Telomeres and telomerase in normal and cancer stem cells. *FEBS Lett*. 2010;584(17):3819–3825.
13. La SH, Kim SJ, Kang HG, Lee HW, Chun KH. Ablation of human telomerase reverse transcriptase (hTERT) induces cellular senescence in gastric cancer through a galectin-3 dependent mechanism. *Oncotarget*. 2016;7(35):57117–57130.
14. Hu C, et al. hTERT promotes the invasion of gastric cancer cells by enhancing FOXO3a ubiquitination and subsequent ITGB1 upregulation. *Gut*. 2017;66(1):31–42.
15. Tang B, et al. Human telomerase reverse transcriptase (hTERT) promotes gastric cancer invasion through cooperating with c-Myc to upregulate heparanase expression. *Oncotarget*. 2016;7(10):11364–11379.
16. Killela PJ, et al. TERT promoter mutations occur frequently in gliomas and a subset of tumors derived from cells with low rates of self-renewal. *Proc Natl Acad Sci U S A*. 2013;110(15):6021–6026.
17. Vinagre J, et al. Frequency of TERT promoter mutations in human cancers. *Nat Commun*. 2013;4:2185.
18. Qu Y, et al. Low frequency of TERT promoter mutations in a large cohort of gallbladder and gastric cancers. *Int J Cancer*. 2014;134(12):2993–2994.
19. Peifer M, et al. Telomerase activation by genomic rearrangements in high-risk neuroblastoma. *Nature*. 2015;526(7575):700–704.
20. Cao Y, Bryan TM, Reddel RR. Increased copy number of the TERT and TERC telomerase subunit genes in cancer cells. *Cancer Sci*. 2008;99(6):1092–1099.
21. Kyo S, Takakura M, Fujiwara T, Inoue M. Understanding and exploiting hTERT promoter regulation for diagnosis and treatment of human cancers. *Cancer Sci*. 2008;99(8):1528–1538.
22. Hu LH, Chen FH, Li YR, Wang L. Real-time determination of human telomerase reverse transcriptase mRNA in gastric cancer. *World J Gastroenterol*. 2004;10(23):3514–3517.
23. Chen F, Hu L, Li Y, Wang L. Expression of telomerase subunits in gastric cancer. *J Huazhong Univ Sci Technol Med Sci*. 2005;25(6):741–743.
24. Gigek CO, et al. hTERT methylation and expression in gastric cancer. *Biomarkers*. 2009;14(8):630–636.
25. Guo YA, et al. Mutation hotspots at CTCF binding sites coupled to chromosomal instability in gastrointestinal cancers. *Nat Commun*. 2018;9(1):1520.
26. Lebel R, McDuff FO, Lavigne P, Grandbois M. Direct visualization of the binding of c-Myc/Max heterodimeric b-HLH-LZ to E-box sequences on the hTERT promoter. *Biochemistry*. 2007;46(36):10279–10286.
27. O'Hagan RC, et al. Gene-target recognition among members of the myc superfamily and implications for oncogenesis. *Nat Genet*. 2000;24(2):113–119.
28. Liao D. Emerging roles of the EBF family of transcription factors in tumor suppression. *Mol Cancer Res*. 2009;7(12):1893–1901.
29. Neve RM, et al. A collection of breast cancer cell lines for the study of functionally distinct cancer subtypes. *Cancer Cell*. 2006;10(6):515–527.
30. GTEx Consortium. Human genomics. The Genotype-Tissue Expression (GTEx) pilot analysis: multitissue gene regulation in humans. *Science*. 2015;348(6235):648–660.
31. Duff MO, et al. Genome-wide identification of zero nucleotide recursive splicing in Drosophila. *Nature*. 2015;521(7552):376–379.
32. Fagerberg L, et al. Analysis of the human tissue-specific expression by genome-wide integration of transcriptomics and antibody-based proteomics. *Mol Cell Proteomics*. 2014;13(2):397–406.
33. Nanki K, et al. Divergent routes toward Wnt and R-spondin niche independency during human gastric carcinogenesis. *Cell*. 2018;174(4):856–869.e17.
34. Viré E, et al. The Polycomb group protein EZH2 directly controls DNA methylation. *Nature*. 2006;439(7078):871–874.
35. Varambally S, et al. The polycomb group protein EZH2 is involved in progression of prostate cancer. *Nature*. 2002;419(6907):624–629.
36. Guerra JVDS, et al. Genes Controlled by DNA Methylation Are Involved in Wilms Tumor Progression. *Cells*. 2019;8(8):E921.
37. Martino D, et al. Epigenome-wide association study reveals longitudinally stable DNA methylation differences in CD4$^+$ T cells from children with IgE-mediated food allergy. *Epigenetics*. 2014;9(7):998–1006.
38. Shao L, et al. Methylation of the HOXA10 promoter directs miR-196b-5p-dependent cell proliferation and invasion of gastric cancer cells. *Mol Cancer Res*. 2018;16(4):696–706.
39. Lauffer BE, et al. Histone deacetylase (HDAC) inhibitor kinetic rate constants correlate with cellular histone acetylation but not transcription and cell viability. *J Biol Chem*. 2013;288(37):26926–26943.
40. Jung I, et al. A compendium of promoter-centered long-range chromatin interactions in the human genome. *Nat Genet*. 2019;51(10):1442–1449.
41. Huang FW, Hodis E, Xu MJ, Kryukov GV, Chin L, Garraway LA. Highly recurrent TERT promoter mutations in human melanoma. *Science*. 2013;339(6122):957–959.
42. McLean CY, et al. GREAT improves functional interpretation of *cis*-regulatory regions. *Nat Biotechnol*. 2010;28(5):495–501.
43. Treiber N, Treiber T, Zocher G, Grosschedl R. Structure of an Ebf1:DNA complex reveals unusual DNA recognition and structural homology with Rel proteins. *Genes Dev*. 2010;24(20):2270–2275.
44. Landt SG, et al. ChIP-seq guidelines and practices

of the ENCODE and modENCODE consortia. *Genome Res*. 2012;22(9):1813–1831.

45. Heinz S, et al. Simple combinations of lineage-determining transcription factors prime cis-regulatory elements required for macrophage and B cell identities. *Mol Cell*. 2010;38(4):576–589.
46. Muratani M, et al. Nanoscale chromatin profiling of gastric adenocarcinoma reveals cancer-associated cryptic promoters and somatically acquired regulatory elements. *Nat Commun*. 2014;5:4361.
47. Farh KK, et al. Genetic and epigenetic fine mapping of causal autoimmune disease variants. *Nature*. 2015;518(7539):337–343.
48. Yan T, et al. HoxC5 and miR-615-3p target newly evolved genomic regions to repress hTERT and inhibit tumorigenesis. *Nat Commun*. 2018;9(1):100.
49. Kim NW, et al. Specific association of human telomerase activity with immortal cells and cancer. *Science*. 1994;266(5193):2011–2015.
50. Jin F, et al. A high-resolution map of the three-dimensional chromatin interactome in human cells. *Nature*. 2013;503(7475):290–294.
51. Yao X, et al. *VHL* Deficiency drives enhancer activation of oncogenes in clear cell renal cell carcinoma. *Cancer Discov*. 2017;7(11):1284–1305.
52. Platt JL, et al. Capture-C reveals preformed chromatin interactions between HIF-binding sites and distant promoters. *EMBO Rep*. 2016;17(10):1410–1421.
53. Barthel FP, et al. Systematic analysis of telomere length and somatic alterations in 31 cancer types. *Nat Genet*. 2017;49(3):349–357.
54. Liberg D, Sigvardsson M, Akerblad P. The EBF/Olf/Collier family of transcription factors: regulators of differentiation in cells originating from all three embryonal germ layers. *Mol Cell Biol*. 2002;22(24):8389–8397.
55. Boller S, Grosschedl R. The regulatory network of B-cell differentiation: a focused view of early B-cell factor 1 function. *Immunol Rev*. 2014;261(1):102–115.
56. Jimenez MA, Akerblad P, Sigvardsson M, Rosen ED. Critical role for Ebf1 and Ebf2 in the adipogenic transcriptional cascade. *Mol Cell Biol*. 2007;27(2):743–757.
57. Gao H, et al. Early B cell factor 1 regulates adipocyte morphology and lipolysis in white adipose tissue. *Cell Metab*. 2014;19(6):981–992.
58. Garel S, Marín F, Grosschedl R, Charnay P. Ebf1 controls early cell differentiation in the embryonic striatum. *Development*. 1999;126(23):5285–5294.
59. Fernandez-Jimenez N, et al. Lowly methylated region analysis identifies EBF1 as a potential epigenetic modifier in breast cancer. *Epigenetics*. 2017;12(11):964–972.
60. Armartmuntree N, et al. Prolonged oxidative stress down-regulates Early B cell factor 1 with inhibition of its tumor suppressive function against cholangiocarcinoma genesis. *Redox Biol*. 2018;14:637–644.
61. Huang KK, et al. Genomic and epigenomic profiling of high-risk intestinal metaplasia reveals molecular determinants of progression to gastric cancer. *Cancer Cell*. 2018;33(1):137–150.e5.
62. Goh AM, Coffill CR, Lane DP. The role of mutant p53 in human cancer. *J Pathol*. 2011;223(2):116–126.
63. Roadmap Epigenomics Consortium, et al. Integrative analysis of 111 reference human epigenomes. *Nature*. 2015;518(7539):317–330.
64. Xu Y, Goldkorn A. Telomere and telomerase therapeutics in cancer. *Genes (Basel)*. 2016;7(6):E22.
65. Chiappori AA, et al. A randomized phase II study of the telomerase inhibitor imetelstat as maintenance therapy for advanced non-small-cell lung cancer. *Ann Oncol*. 2015;26(2):354–362.